Master's Thesis in Climate Dynamics

Dense water formation in the Greenland Sea between 1999 and 2009

Kristin Svingen

August 1, 2019

Geophysical institute
University of Bergen

Abstract

A 10-year continuous hydrographic data record from moored profilers located in the central Greenland Sea between 1999 and 2009 were used to examine the mixed-layer depth evolution through winter as well as interannual variability in water column properties and convection depth. The water column has become significantly warmer and more saline through the decade. The depth of convection each winter was a result of heat loss to the atmosphere, the water column stratification, and lateral fluxes of heat and salt. Even though the mixed-layer depth differed from year to year the evolution through each winter showed a similar pattern which could be separated into three distinct phases. Most of the mixed-layer cooling took place during the first phase. In the second phase the mixed layer deepened rapidly before it stabilized and restratified in the third phase at the end of the winter. The high temporal resolution of the data set allowed for a detailed investigation of the mixed layer and its direct response to atmospheric forcing on short time scales. The effect of short, intense atmospheric events, called cold air outbreaks, on the mixed layer depended strongly on which phase they occurred within. While strong atmospheric forcing in the first phase of the convection process mainly cooled the mixed layer, it led to a significant mixed-layer deepening during the second phase. Experiments done with a one-dimensional mixed-layer model suggested that intense events of heat loss early in winter are more favorable for deep convection to occur.

Acknowledgments

First of all I want to thank my supervisor, Kjetil Våge, for giving me the opportunity to write my thesis about this interesting topic. Thank you for all the helpful feedback, good advice, and guidance. I really appreciate the time and effort you have given me and this project. Thank you also for giving me the opportunity to participate in an exciting research cruise to the Iceland Sea. That was a great experience I will never forget. I would also like to thank my co-supervisor, Ailin Brakstad, for all the support, motivation and help. Thank you for always having the door open for me and all my small and big problems. Thanks to Gereon Budéus and the Alfred Wegener Institute for providing the mooring data. Thanks to Lukas Papritz for help with downloading atmospheric data and for helpful inputs. Thanks also to the entire OVENS group for interesting group meetings through the last two years, I have learned so much from you. In particular thanks to Stefanie Semper who introduced me to the OVENS group in the first place.

Finally, thanks to my friends and family for all the support on the way. Thanks to my parents for always being just a phone call away. Thanks to my aunt and uncle, Ingunn and Vegard, for all the encouragement, and all the food, you have given me during my five years in Bergen. Last, but not least, thanks to my fellow students at GFI for making these five years unforgettable. In particular thanks to those I have shared Odd with the last year. Long days (and nights) in the study hall have been almost no problem together with you, extreme amounts of coffee and endless rounds of playing Ligretto.

Contents

Chapter 1

Introduction and background

1.1 The Atlantic Meridional Overturning Circulation

The Atlantic Meridional Overturning Circulation (AMOC) plays a crucial role in global climate. Along with the atmospheric circulation it is responsible for the meridional transport of heat from equator toward higher latitudes (Dickson and Brown, 1994; Rhines et al., 2008). Much attention has been drawn to the AMOC and its response to the warming climate. Recent direct measurements of the circulation show large variability in AMOC volume transport (Lozier et al., 2019; Srokosz and Bryden, 2015) and the fifth assessment report of the Intergovernmental Panel on Climate Change (IPCC) projected a weakening in the AMOC over the 21st century (IPCC, 2014). Based on data from an array of moorings spanning the Atlantic at 26 °N, Smeed et al. (2018) found that the AMOC has slowed down after 2008. Østerhus et al. (2019), on the other hand, found no evidence for such a weakening further north in the overturning in the Nordic Seas.

The upper branch of the AMOC transports warm and saline Atlantic Water (AW) northward. On its way north, heat is lost to the atmosphere, and the water becomes dense and sinks. This transformation produces colder deep and intermediate water masses that supply the lower branch of the circulation which returns to the south at depth (Dickson and Brown, 1994; Marshall and Schott, 1999). To close the overturning loop, the water is brought back to the surface through diapycnal mixing (mixing across surfaces of equal density) in the ocean interior or by wind-driven upwelling in the Southern Ocean (Kuhlbrodt et al., 2007). The dense water formation at high latitudes does not supply energy to the system, but the amount of dense water that is produced is of great importance in determining the strength and spatial distribution of the AMOC (Kuhlbrodt et al., 2007). In the North Atlantic dense water formation takes place in the Labrador, Irminger, and Nordic Seas. Lozier et al. (2019) found that the Labrador Sea does not play a key role for the water mass transformation and that most of the conversion from light to dense water occurs east of Greenland. This was corroborated by Chafik and Rossby (2019) who concluded that water mass transformation in the Nordic Seas accounts for most of the overturning circulation.

1.2 The Nordic Seas

The Nordic Seas is a collective term for the Norwegian, Greenland, and Iceland Seas, and are separated from the North Atlantic by the Greenland-Scotland Ridge (GSR, Figure 1.1). The deepest gaps in the GSR are the 840 m deep Faroe Bank Channel (FBC) and Denmark Strait which has a sill depth of 630 m (Hansen and Østerhus, 2000). Below these depths, the ridge serves as a solid barrier between the Nordic Seas and the North Atlantic. At the surface warm and saline AW enters the Nordic Seas in an extension of the Gulf Stream an in the North Icelandic Irminger Current (NIIC) which flows northward east and west of Iceland, respectively. AW is modified north of GSR and the resulting product spills southward through gaps in the ridge as overflow plumes that sink into the abyss of the North Atlantic. This overflow water is generally defined by a potential density greater $\sigma_\theta = 27.8$ kgm^{-3} (Dickson and Brown, 1994).

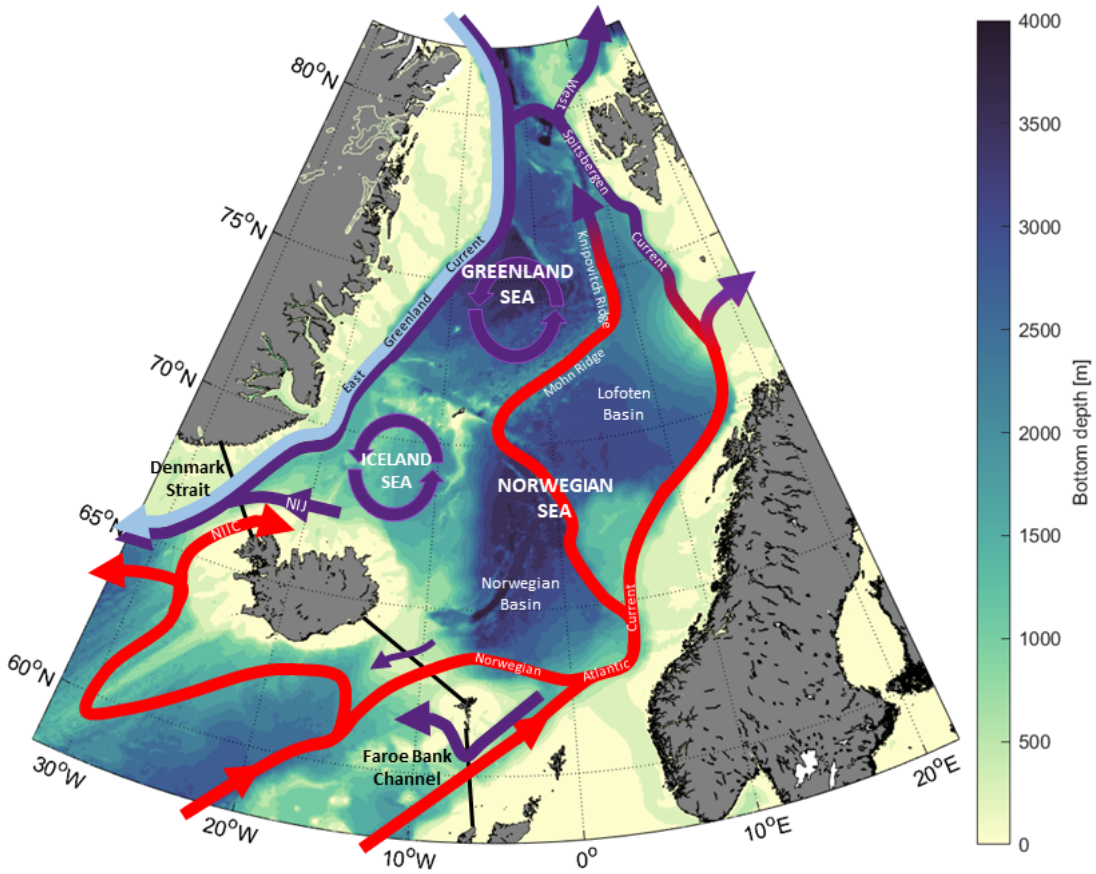

Figure 1.1: Map over the Nordic Seas showing bathymetry and general circulation pattern. Red arrows represent currents of warm and saline Atlantic Water, while arrows colored dark purple indicate dense and cold water. The cyclonic gyre circulations in the Greenland and Iceland Seas are illustrated in purple. Light blue indicates cold and fresh Polar Surface Water. The GSR is marked by the black line. NIJ and NIIC are acronyms for the North Icelandic Jet and the North Icelandic Irminger Current, respectively.

The Greenland and Iceland Seas are situated in the western part of the Nordic Seas, separated from the Norwegian Sea by the Jan Mayen, Mohn, and Knipovich Ridges. The two basins are separated from each other by the West Jan Mayen Ridge. To the north, the Greenland Sea is connected with the Arctic Ocean through Fram Strait. Both the Greenland and Iceland Seas are characterized by cyclonic gyre circulations. The Greenland and Iceland Seas combined are referred to as te Arctic domain and are confined by strong hydrographic fronts both to the west and east (Swift and Aagaard, 1981). The Polar Front separates the gyres from the relatively colder and fresher Polare Surface Water (PSW) in the Polar domain to the west. PSW flows southward at the surface from the Arctic in the East Greenland Current (EGC). To the east of the Arctic domain, the Arctic Front forms the border toward the much warmer and more saline AW in the Atlantic domain which covers the eastern part of the Nordic Seas.

The largest inflow of AW into the Nordic Seas occurs east of Iceland (Østerhus et al., 2019). After the extension of the Gulf Stream have crossed GSR it becomes the Norwegian Atlantic Current (NwAC). The NwAC follows the continental slope of Norway northward until it separates into two branches. The inner branch of the NwAC continues along the west coast of Norway, while the outer NwAC branch follows the Mohn and Knipovich Ridges. On its way northward the AW is modified through heat loss to the atmosphere and by mixing with ambient water and becomes colder and fresher (Mauritzen, 1996). While one part of the inner NwAC enters the Barents Sea and subsequently the Arctic Ocean, another portion continues toward Fram Strait along the west coast of Svalbard as the West Spitsbergen Current (WSC). At Fram Strait the densified AW encounters the cold and fresh PSW, and because the modified AW now is denser than the PSW it subducts. One portion of the WSC flows northward through Fram Strait and continues into the Arctic Ocean. The other part of the current recirculates within Fram Strait, joins the EGC, and flows southward along the continental slope of Greenland toward Denmark Strait.

In the eastern part of Denmark Strait, the northward flowing NIIC accounts for a significantly smaller portion of the AW inflow to the Nordic Seas than the inflow east of Iceland. Våge et al. (2011) hypothesized that the NIIC serves as the upper limb in a local overturning cell in the Iceland Sea where the lower limb is the North Icelandic Jet (NIJ) which flows toward Denmark Strait along the Icelandic continental slope (Våge et al., 2011). On the western side of Denmark Strait, PSW exits the Nordic Seas in the EGC. Both EGC and NIJ transport sufficiently dense water masses ($\sigma_\theta > 27.8$ kgm^{-3}) to contribute to the Denmark Strait Overflow Water (DSOW, Harden et al., 2016; Mastropole et al., 2017). DSOW accounts for approximately half of the total dense overflow transport across the GSR. The other half spills over the ridge on the eastern side of Iceland. The largest overflow plume east of Iceland is the FBC overflow water which accounts for one third of the total overflow transport (Hansen et al., 2016; Østerhus et al., 2019).

1.3 Sources and pathways of overflow water

The gradual cooling and densification of AW flowing around the rim of the Nordic Seas and open ocean convection in the Greenland and Iceland Seas are the main sources of overflow water in the

Nordic Seas. Overflow water formed in the Greenland and Iceland Seas is termed Arctic-origin water, while the resulting product of the gradually modified AW primarily formed in the eastern part of the Nordic Seas is referred to as Atlantic-origin. Through the last decades, the relative importance of these two main sources for overflow water and their pathways in the Nordic Seas have been under debate.

1.3.1 Overflow west of Iceland

In the 19080s and the early 1990s open ocean convection in the western part of the Nordic Seas was thought to be the main source of DSOW and the Iceland Sea was identified as the main site of formation (Swift et al., 1980; Swift and Aagaard, 1981; Strass et al., 1993). Mauritzen (1996), however, discarded this hypothesis. One of her arguments for excluding the Iceland Sea as a main source region was the lack of a direct pathway from the formation site toward the sill. Instead, Mauritzen (1996) suggested an alternative overturning circulation scheme where the gradual transformation of AW as it flows around the rim of the Nordic Seas is the main source of DSOW. Eldevik et al. (2009) found that approximately 64 % of the DSOW is Atlantic-origin water and supported the scheme of Mauritzen (1996). In addition, 31 % of the DSOW can be traced back to the convective basins in the western Nordic Seas according to Eldevik et al. (2009).

In the early 2000s the Iceland Sea regained attention as a possible source region for DSOW. Jónsson and Valdimarsson (2004) discovered a current transporting overflow water along the slope north of Iceland into Denmark Strait. This current was later named the North Icelandic Jet (NIJ, Våge et al., 2011). Further investigation of the current revealed that the water transported by the NIJ can account for roughly one third of the total DSOW transport, including nearly all of the densest portion of the overflow water ($\sigma_\theta > 28.03$ kgm^{-3}, Våge et al., 2011; Harden et al., 2016). However, from historical records Våge et al. (2015) demonstrated that only very occasionally mixed layers within the Iceland Sea were denser than $\sigma_\theta = 28.03$ kgm^{-3}. The product of wintertime convection in the Iceland Sea can therefore not be the main source of the densest portion of DSOW. Instead, Våge et al. (2015) hypothesized that the densest portion of DSOW originates in the Greenland Sea. This is supported by Brakstad et al. (2019) who found that the density of intermediate water masses formed in the Greenland Sea gyre during winter generally exceeds $\sigma_\theta = 28.03$ kgm^{-3}. Messias et al. (2008) also found evidence that there is rapid transport of intermediate water masses from the Greenland Sea to the Iceland Sea.

Today the general understanding is that there are two main pathways supplying DSOW. Two thirds of the overflow is of Atlantic-origin which is gradually densified in the boundary current system and transported toward the strait by the EGC. The remaining third is of Arctic-origin, formed by open ocean convection in the Iceland and Greenland Seas, and transported toward the strait primarily by the NIJ.

1.3.2 Overflow east of Iceland

The Faroe Bank Channel Overflow Water (FBCOW) is the second largest contributor to the lower limb of the AMOC and the most important overflow branch east of Iceland. Overflow across other regions between Iceland and Scotland (the Wyville Thomson Ridge and the Iceland-Faroe Ridge) are significantly weaker (Østerhus et al., 2019). FBCOW includes the densest water that passes over the GSR. However, because of entrainment and mixing with ambient water masses after crossing the sill, the end product becomes both warmer and fresher and is less dense than the DSOW (Hansen et al., 2016; Fogelqvist et al., 2003).

According to Fogelqvist et al. (2003) FBCOW is a mixture of Norwegian Sea Deep Water and Norwegian Sea Arctic Intermediate Water (NSDW and NSAIW). The intermediate portion (accounting for roughly half the overflow water) is mainly a product of wintertime convection in the Greenland Sea. Jeansson et al. (2017) confirmed that intermediate water masses from the Greenland and Iceland Seas are important contributors to the NSAIW. The intermediate water formed in the Greenland Sea contributes with 50 % of the NSAIW with densities greater than $\sigma_\theta = 28.04$ kgm^{-3}. This composition of overflow water is also supported by Eldevik et al. (2009), who found found that 61 % of the FBCOW consists of water originating in the Arctic domain.

This suggests that intermediate water formed in the Greenland Sea is of importance to the AMOC through its contributions to the GSR overflows both west and east of Iceland. The densest portion of the overflow water, in particular, largely originates in the Greenland Sea.

1.4 Open ocean convection in the Greenland Sea

During open ocean convection, surface water masses are mixed to depth and the upper part of the water column is homogenized. For this to occur, strong buoyancy loss at the surface and a weakly stratified water column are required. A cyclonic gyre circulation, such as the circulation in the Greenland Sea, is favorable for open ocean convection because it leads to divergence in the surface and consequently a doming of the underlying isopycnals which brings weakly stratified water closer to the surface. Below the surface, mixing by deep convection previous winters has preconditioned the water column by reducing the vertical density gradients and weakened the water column stability (Marshall and Schott, 1999). When the weakly stratified water is brought closer to the surface, it is more accessible for atmospheric forcing. The stability of the water column is given by the buoyancy frequency

$$N^2 = -\frac{g}{\rho_0}\frac{\partial \rho}{\partial z} \tag{1.1}$$

where g is the gravitational acceleration, ρ is the density, and ρ_0 is a constant reference density set to 1000 kgm^{-3}. The closer to zero the buoyancy frequency is, the weaker is the stratification. Strong turbulent heat fluxes from the ocean to the atmosphere during winter lead to a cooling and a density increase in the surface layer. The turbulent heat flux is the sum of the sensible and latent heat fluxes. Convection occurs when the surface water becomes sufficiently dense such that

the water column is unstable ($N^2 < 0$) and the surface water overturns in plumes of dense water (Marshall and Schott, 1999). These plumes, with a horizontal scale of less than 1 km, mixes the water column properties in the vertical and occur throughout the entire gyre. The result is a homogeneously mixed patch over the preconditioned site (Marshall and Schott, 1999). Brakstad et al. (2019) demonstrated how both stratification and atmospheric forcing are important for convection to take place in the Greenland Sea. They showed that convection only reached shallow depths during winters when the surface layer the preceding fall was anomalously fresh (and the water column stratification was strong) regardless of the magnitude of the surface heat loss. However, even for weakly stratified water columns, strong heat fluxes were required to obtain deep convection.

Before 1980 convection in the Greenland Sea was considered the main source for deep water in the Nordic Seas. Deep convection, nearly reaching the bottom, formed the very cold and dense Greenland Sea Deep Water (GSDW, Malmberg, 1983; Aagaard et al., 1985). Since the early 1980s no bottom-reaching convection has been observed, and the GSDW has not been ventilated (Meincke et al., 1997; Karstensen et al., 2005; Ronski and Budéus, 2005). Brakstad et al. (2019) found that between 1986 and 1993 the average mixed layer depth did not exceed 300 m. Since the atmospheric forcing was strong these winters, they suggested that the main reason for this shallow convection was a low-salinity layer in the upper part of the water column increasing the stratification and inhibiting deep convection. Budéus et al. (1998) found that an intermediate temperature maximum was established early in the 1990s. This caused a stability maximum separating the intermediate layer from the deep water, preventing convection from reaching the deepest part of the water column (Karstensen et al., 2005; Ronski and Budéus, 2005). After 1993 convection depths have increased and in general exceeded 500 m. The main product of convection in the Greenland Sea since the cessation of deep convection is Greenland Sea Arctic Intermediate Water (GSAIW). This water mass is separated from GSDW by the stability maximum which arose in the early 1990s. GSAIW is both warmer and less saline than GSDW, but is still denser than 28.03 kgm^{-3} and is thus dense enough to contribute to the densest portion of DSOW (Brakstad et al., 2019). Increasing rates of GSAIW formation has deepened the boundary between GSAIW and GSDW, and after 2002 the GSDW had disappeared from the upper 2000 m of the water column (Brakstad et al., 2019).

Since the late 1980s there has been a warming of the entire water column in the Greenland Sea (Østerhus and Gammelsrød, 1999; Latarius and Quadfasel, 2010; Lauvset et al., 2018; Brakstad et al., 2019). According to Latarius and Quadfasel (2010) this change was due to relatively warmer Atlantic-origin water intruding the gyre at intermediate depths. The lateral supply of heat overcompensated for the heat lost to the atmosphere during winter and the result was a net warming. Accompanied by this warming was an increasing trend in salinity (Lauvset et al., 2018; Brakstad et al., 2019). Lauvset et al. (2018) connected the changes in both temperature and salinity to anomalies in the AW inflow that circulates the Nordic Seas and are mixed laterally into the gyre. Both Lauvset et al. (2018) and Brakstad et al. (2019) argued that mixed-layer depths have deepened over the first 10-15 years of the 2000s, despite weaker atmospheric forcing. The primary reason was that increased salinity resulted in weaker stratification and hence a more preconditioned

water column.

Even during winters with high upper ocean salinities and weak stratification, strong atmospheric forcing is required for deep convection to occur (Brakstad et al., 2019). In general the buoyancy loss from the ocean surface is largest in regions along the marginal ice zone where cold, dry winds first encounter open ocean (Moore et al., 2015; Marshall and Schott, 1999). Between 1979 and 2014 the turbulent heat fluxes over the Greenland Sea weakened by approximately 20 % (Moore et al., 2015). This decrease occurred simultaneously with a retreat of the ice edge towards Greenland, which shifted the region of strongest heat fluxes westward. A decreasing temperature difference between the ocean and the atmosphere has also contributed to the weaker heat fluxes. Using a one-dimensional mixed-layer model Moore et al. (2015) showed how such a negative trend in atmospheric forcing has led to diminishing mixed-layer depths. If the reduction of atmospheric forcing continues, they hypothesized that convection in the Greenland Sea may be limited to shallow depths in the future which in turn can weaken the AMOC.

1.5 Cold air outbreaks

In the Nordic Seas cold air outbreaks (CAOs) are responsible for 60-80 % of the total wintertime heat loss from the ocean (Papritz and Spengler, 2017), and are thus of great importance for dense water formation (Dickson et al., 1996). CAOs occur when cold polar air flows over relatively warm water (Papritz and Spengler, 2017) and are generally identified by the potential temperature difference between the sea surface and a reference pressure level in the upper atmosphere (Kolstad et al., 2009; Papritz et al., 2015; Fletcher et al., 2016). The air-sea potential temperature difference ($\theta_{SST} - \theta_p$) is called the CAO-index. Positive indices indicate that the sea surface is warmer than the air masses above, and turbulent heat fluxes are directed from the ocean to the atmosphere. Papritz and Spengler (2017) identified CAO events by the air-sea potential temperature difference $\theta_{SKT} - \theta$, where θ is the potential temperature of an air parcel, and θ_{SKT} is the potential skin temperature. Based on this index Papritz and Spengler (2017) divided CAO events into four intensity classes: weak, moderate, strong, and very strong CAOs. The definition of the intensity classes is shown in Table 1.1.

Table 1.1: CAO intensity classes as defined by Papritz and Spengler (2017)

Intensity class	**CAO-index interval**
Weak	$0K < \theta_{SKT} - \theta \leq 4K$
Moderate	$4K < \theta_{SKT} - \theta \leq 8K$
Strong	$8K < \theta_{SKT} - \theta \leq 12K$
Very strong	$12K < \theta_{SKT} - \theta$

Using wintertime reanalysis data from 1979 to 2014 Papritz and Spengler (2017) found that the occurrence of weak CAOs was mainly dictated by the sea surface temperature (SST). The highest frequencies of weak CAOs were found in the eastern Nordic Seas where the warm AW inflow is situated at the surface. The occurrence of stronger CAOs, on the other hand, did not seem to depend on warm SSTs. Moderate and strong CAOs developed most frequently in a band following the ice edge along the east coast of Greenland and in the Barents Sea. The very strong CAOs were mostly confined to the northern part of the Greenland Sea and Fram Strait. Along the sea ice edge and over the Greenland Sea, moderate to very strong CAOs accounted for roughly 60 % of the total wintertime heat loss (Figure 1.2). It is thus the most intense CAO events that are of primary importance for dense water formation in the western Nordic Seas (Papritz and Spengler, 2017).

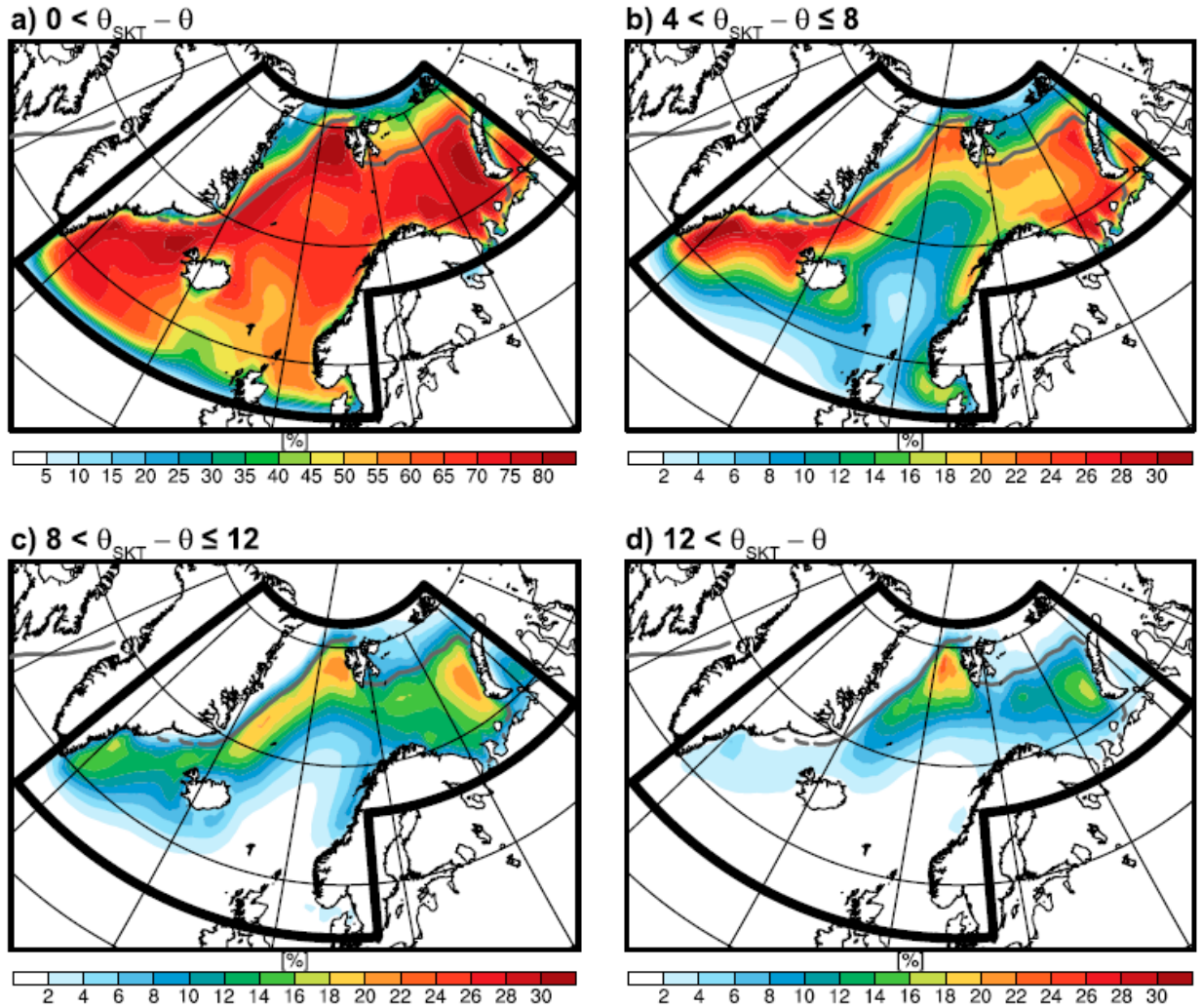

Figure 1.2: Percentage of ocean to atmosphere surface turbulent heat flux associated with CAO events (a) for all events and (b)-(d) for moderate, strong, and very strong events, respectively. The mean sea ice edge is illustrated by the 50 % sea ice concentration contour in gray. (Figure 10 from Papritz and Spengler, 2017)

The contribution of CAOs to the total heat loss is most pronounced close to the ice edge (Figure 1.2). Våge et al. (2015) showed that the deepest convection in the Iceland Sea takes place in the north-western part of the basin, away from the center of the gyre, because of stronger atmospheric forcing near the ice edge. Even though the strongest heat fluxes are found close to the ice edge also in the Greenland Sea, Brakstad et al. (2019) documented that the deepest mixed layers were confined to the center of the gyre. Since the Greenland Sea has steeper topography around the rim of the gyre and stronger wind forcing than the Iceland Sea, the gyre circulation is stronger in the Greenland Sea (Voet et al., 2010). In addition the surface heat fluxes are stronger in the Greenland Sea than in the Iceland Sea (Moore et al., 2015). The combination of a stronger gyre and higher heat fluxes makes the Greenland Sea more prone to deep convection than the Iceland Sea and the location of the deepest convection is hence less dependent on the ice edge location.

1.6 Motivation for this study

Water mass transformation in the Greenland Sea has been an active topic of investigation over the last decades (e.g. Ronski and Budéus, 2005; Latarius and Quadfasel, 2010, 2016; Brakstad et al., 2019). Because of sparse data coverage, these studies have mainly focused on the interannual variability in end-of-winter convection depth. In this study we want to investigate the evolution of the mixed layer through the winter more thoroughly. Such a detailed investigation is made possible by the high temporal resolution of data obtained from moored profilers located within the gyre between 1999 and 2009. The high temporal resolution also allows for investigation of the response of the mixed layer to atmospheric forcing on short time scales. The impact of CAOs is in particular examined. CAOs account for most of the atmospheric heat loss in the Greenland Sea (Papritz and Spengler, 2017), and Moore et al. (2015) and Somavilla (2019) indicated that the strength and frequency of CAOs will decrease in the future. Hence, it is important to understand the impact of CAOs for future development of the mixed layer in the Greenland Sea.

Chapter 2

Data and methods

2.1 Hydrographic data

Between 1999 and 2009 three moored profilers were deployed annually in the central Greenland Sea. The locations of the moorings, hereafter referred to as mooring A, B, and C, respectively, are given in Table 2.1 and shown in Figure 2.1. Each profiler was equipped with a SeaBird Electronics Seacat SBE 19plus that measured conductivity, temperature, and depth (CTD). The accuracy of the instrument was 0.005°C for temperature and 0.0005 S/m for conductivity. For the observed temperature range, this corresponds to a salinity accuracy smaller than 0.01. Each summer the moorings were recovered and data were downloaded before the moorings were redeployed. In order to profile to the bottom of the water column the profiler had to be nearly neutrally buoyant. This was challenging near the surface where the stratification was high and there was strain on the mooring due to waves. The moorings therefore only profiled from approximately 100 m to the bottom (Budéus, 2009). The starting point of the profiles was constant through each individual winter, but varied from 95 to 185 m over the deployment period.

In addition to these three moorings, a supplementary mooring was deployed the last year (2008/2009). This mooring was located 1.8 km away from mooring C and provided measurements from the surface to 130 m depth. To withstand the influence of surface waves, this mooring was equipped with a heavier profiler than the other moorings. The profiler on this mooring was equipped with a SeaBird Electronics SBE41, which has an accuracy of 0.002°C and 0.002 for temperature and salinity, respectively. Measurements from moorings B and C were combined with surface measurements from the supplementary mooring to form profiles from the bottom to the surface. The transition between the two data sets was not smoothed and the profiles from 2008/2009 are hence characterized by a distinct joint at 130 m. Details about the deployment from 2008/2009 can be found in a technical report (Budéus, 2009).

Table 2.1: Locations of the moorings

Mooring	Longitude	Latitude
A	2°30' W	74°50' N
B	3°27' W	75°05' N
C	4°37' W	74°55' N

Vertical CTD profiles were generally obtained every second day, except during 2008/2009 when daily profiles were collected. However, due to technical problems there were several periods where one or more of the moored profilers were parked at a constant depth. These periods with missing profiles were either entire deployments where the profiler did not function or shorter periods throughout the year when profiling was prevented by strong currents (Budéus, 2009).

Post processed mooring data were provided by Dr. Gereon Budéus (Alfred Wegener Institute for Polar and Marine Research). The post processing included calibration of the moored profilers against shipboard CTD measurements each year, smoothing of the profiles with a median filter, and interpolation of the data to integer pressure values. Additional quality control was performed by excluding all values outside the expected range of temperature and salinity in the Nordic Seas of [-2°C,20°C] and [20,36], respectively. Casts where the moored profilers were parked at constant depth were removed from the data set. The total data coverage from each mooring after the quality control was carried out is shown in Figure 2.2.

Following the new standard of the International Thermodynamic Equation Of Seawater - 2010 (TEOS-10, IOC et al., 2010) conservative temperature and absolute salinity were calculated and used in the analysis. As opposed to practical salinity, which depends on the conductivity of seawater, absolute salinity is directly influenced by the mass of dissolved material in the water. As such, the absolute salinity takes the spatial variations in composition of the seawater into account.

In addition to data from the three moorings wintertime mixed-layer depths determined by Brakstad et al. (2019) were used (Figure 2.1). These were estimated based on hydrographic data collected by shipboard CTDs, autonomous profiling floats, and instrumented seals between 1986 and 2016. The white contour in Figure 2.1 outlines the cyclonic Greenland Sea Gyre as defined by Moore et al. (2015) using the dynamic topography of the surface relative to 500 m. All of the profiling moorings were located within the gyre which coincides with the area where Brakstad et al. (2019) found the deepest and densest convection.

2.2 Mixed-layer depth

Since the moored profilers most years only reached up to approximately 100 m (Section 2.1), only mixed layers extending below this depth could be identified. The exception was the winter of

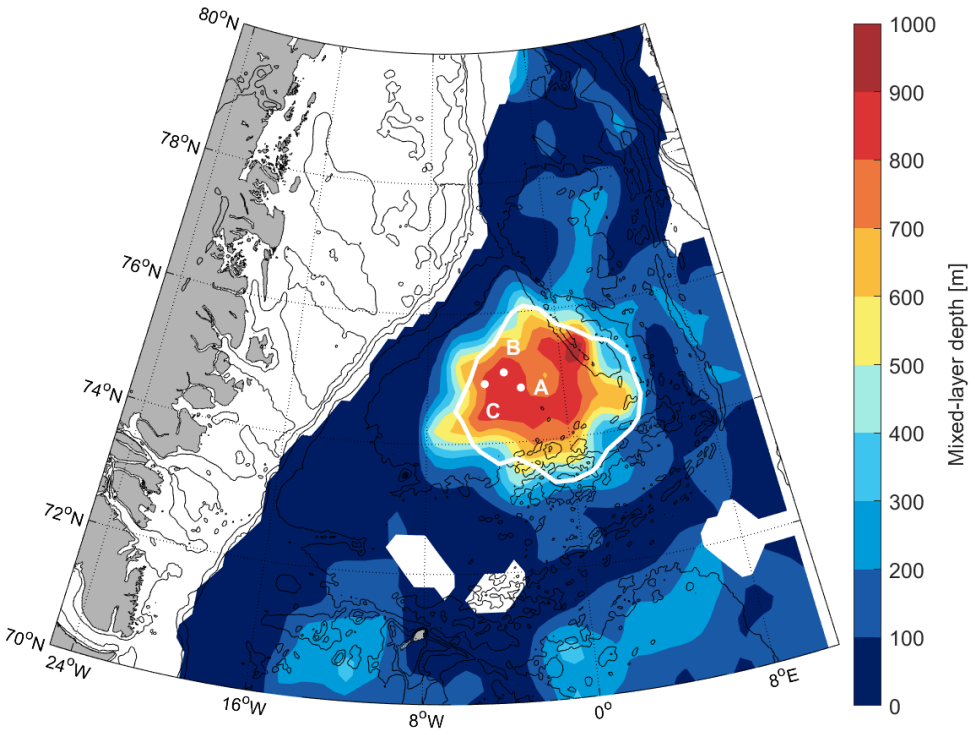

Figure 2.1: Mean late-winter (February-April) mixed-layer depth from the winters with the 30 % deepest convection depths between 1986 and 2016. Locations of the three moorings and the outline of the Greenland Sea Gyre are indicated by the white dots and line, respectively. The black lines show the 250, 500, 1000, 2000, and 3000 m isobaths. The figure is based on Figure 3c in Brakstad et al. (2019).

2008/2009 when data from the supplementary mooring extended the measurements to the surface. In total, mixed layers were identified in 49 % of the profiles. The remaining profiles, without discernible mixed layers, were mainly from summer when the mixed layer was too shallow to detect by the moorings.

For each profile depth and properties of the mixed layer were determined using a procedure previously applied by Våge et al. (2015) and Brakstad et al. (2019). This procedure is based on visual inspection of every hydrographic profile. Two automated routines estimated the mixed-layer depth, employing a curvature and a density difference criterion, respectively. The curvature method, developed by Lorbacher et al. (2006), identified the base of the mixed layer as the shallowest depth where the temperature profile has a curvature extremum. The density difference method, on the other hand, identified the base of the mixed layer as the depth where the increase in potential density from its surface value corresponded to a given ΔT change in temperature (Nilsen and Falck, 2006). Brakstad et al. (2019) argued that because of the weak stratification in the Greenland Sea, $\Delta T = 0.2$ °C is an appropriate threshold. This limit is also used in this study.

Each profile and the depth of the mixed layer estimated by both of the automated routines

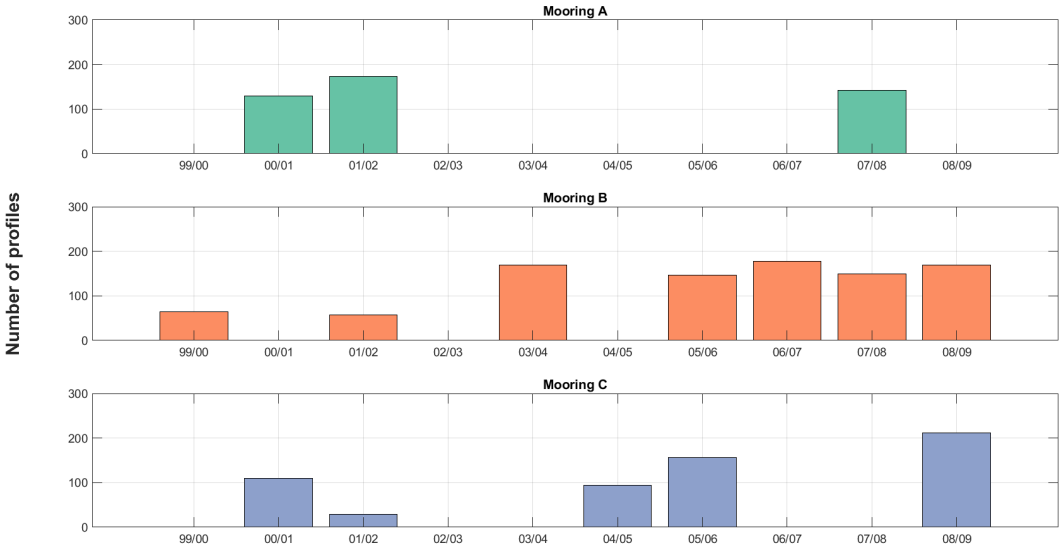

Figure 2.2: Annual number of profiles per deployment at each mooring site.

were then visually inspected. For approximately half of the profiles where the mixed layer was detected by the mooring, one or both of the automated routines accurately estimated the mixed-layer depth. For the remaining profiles, a manual procedure developed by Pickart et al. (2002) was applied. The top and base of the mixed layer were first estimated visually and the means and standard deviations of the mixed-layer temperature, salinity, and density were calculated over this depth range. Finally, the top and bottom of the mixed layer were determined as the depths where the density profile permanently exceeded two standard deviations from the mean. As pointed out by both Våge et al. (2015) and Brakstad et al. (2019), the automated routines were most accurate for strongly stratified profiles where the density gradient between the mixed layer and the deeper part of the water column was pronounced. This is typical for early fall profiles in the Greenland Sea. During winter the density difference is generally smaller and the automated routines less accurate. In addition, the automated routines were not able to detect mixed layers that were separated from the surface either because of early stages of restratification or advection of lighter water masses (see also Section 2.4).

The manual procedure was also employed for most of the profiles from the last year since this data set was constructed from a combination of data from two independent moorings with a distinct joint at 130 m (Section 2.1). When the mixed layer extended beneath the shallow moored profiler, the manual procedure was used to set the upper limit of the mixed layer below the joint, even though the mixed layer extended to the surface. Due to the lateral displacement of the two moorings the hydrographic properties differed slightly. By employing the manual procedure we ensured that mixed-layer properties were estimated based on data only from the deep moored profiler. When the mixed layer was shallower than 130 m and fully detected by the shallow moored profiler, the automated routines generally performed well. In total, approximately half of the identified mixed layers were determined by an automated routine while the rest were determined manually.

2.3 Comparison of mooring data

Although the three moorings were separated by 30-60 km, they were all located within the Greenland Sea Gyre where the deepest convection takes place (Figure 2.1). The evolution of mixed-layer properties at each mooring location were compared to decide whether they could be used interchangeably to describe the general evolution within the gyre.

Time series of mixed-layer depths at each of the three mooring locations for the entire record are shown in Figure 2.3. The variability in depth of the mixed layer was large on short time scales. However, based on winters when data were collected simultaneously by more than one mooring (marked by black lines in Figure 2.3), the end-of-winter mixed-layer depths were in good agreement. The winters of 2007/2008 and 2008/2009 had relatively deep convection (to between 1600 and 1800 m at all mooring locations). In 2005/2006 data from moorings B and C showed slightly shallower convection (to about 800 m), and in 2000/2001 convection at moorings A and C reached approximately 1100 m. In 2001 two of the mixed layers were identified as outliers. These profiles were obtained within a so-called chimney. A chimney is a small-scale vortex, ranging from 5-20 km in diameter, which is characterized by a cold, fresh and weakly stratified core. Chimneys have on several occasions been observed reaching extensively deeper than the general mixed layer in the Greenland Sea (Rudels et al., 1989; Gascard et al., 2002; Wadhams et al., 2002). The profiles obtained within a chimney were not included in the analysis. Despite substantial differences between the moorings on short time scales, the resulting depths of convection each winter agreed well between the different sites.

While some months stood out, the differences in monthly mean mixed-layer properties between the moorings were generally small (Figure 2.4). The largest discrepancies in mixed-layer depth typically occurred in late winter (March and April). This might partially be explained by different onset of restratification at the different mooring location, or by the occurrence of meso-scale eddies that were advected past the moorings (Latarius and Quadfasel, 2010). Passing eddies, carrying warm and saline Atlantic-origin water, caused a pronounced shallowing of the mixed-layer when passing a mooring. Higher frequencies of such eddies at one mooring site would therefore reduce the monthly averaged mixed-layer depth significantly compared to the other. The reason for the large differences in monthly mean mixed-layer depth in April 2009 (almost 700 m) was a combination of the two. The water column restratified mid-April at mooring B while the restratification occurred after April at mooring C and did not affect the monthly mean. The sampling rate was in addition much lower at mooring B than at mooring C. 7 profiles were obtained at mooring B in April 2009, while 17 profiles were obtained at mooring C. Profiles wit a shallow mixed layer due to warm intrusions near the surface therefore influence the monthly mean more at mooring B than at mooring C.

The largest differences in hydrographic properties occurred in early winter (October - Decem-

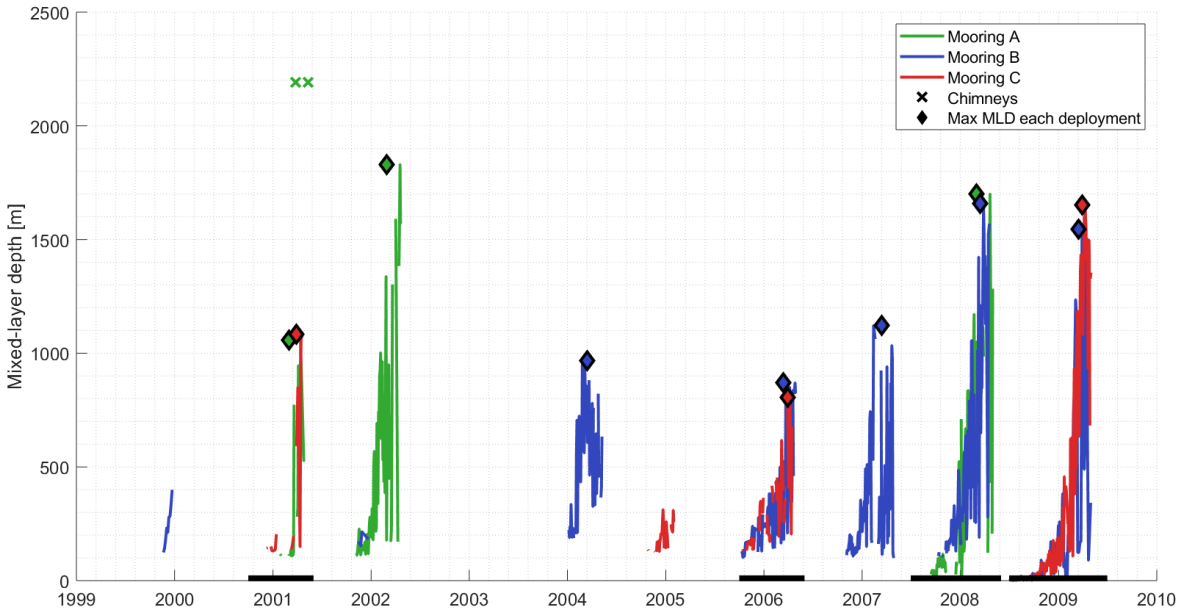

Figure 2.3: Mixed-layer depths between 1999 and 2009. The three moorings are distinguished by different colors. Time periods when data were obtained from multiple moorings are indicated with a black line. The maximum mixed-layer depth for each winter is marked with diamonds (only for years when data from March and April were available). The crosses indicate mixed-layer depths for profiles within a chimney.

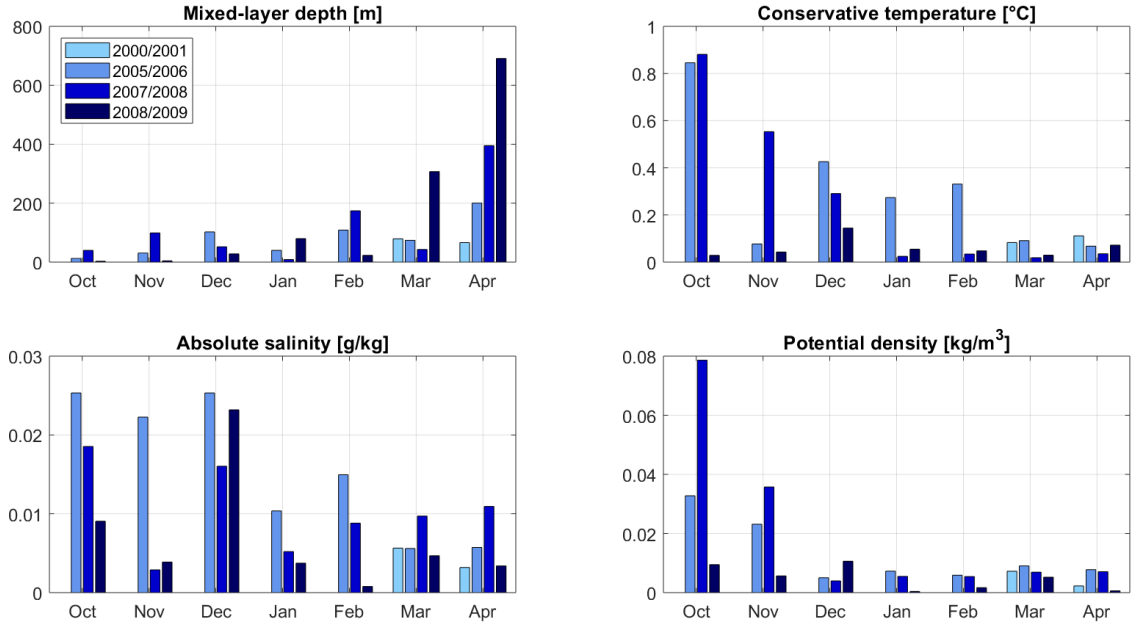

Figure 2.4: Absolute differences in monthly mean mixed-layer properties from winters when data from separate mooring sites overlapped (periods marked by black line in Figure 2.3).

ber) when the mixed layer was shallow (Figure 2.3). As less surface forcing is needed to modify the hydrographic properties of shallow mixed layers, they are generally more variable than the

deeper mixed layers later in winter. The small differences in hydrographic properties at the end of winter (March and April) indicate that the resulting densified water mass varied little between the mooring sites.

A similar analysis was carried out on the hydrographic properties at 2000 m. Throughout the record, the mixed layer never reached 2000 m apart from the two profiles within the chimney. Hence, the water mass properties at this depth were not affected by convection and showed little temporal variability. The differences between the moorings in temperature, salinity, and density at 2000 m were considerably (one order of magnitude) lower than in the mixed layer (not shown).

Since the general evolution and end result of convection (both depth and hydrographic properties) were in good agreement, and the properties below convection depth varied little between the moorings, the data from the three different locations are hereafter used interchangeably in the analysis. Whenever data from the moorings were combined, the independent moorings were marked. Data from mooring B were used as basis for the combined time series. Data gaps were filled using data from the other two moorings.

2.4 Warm surface intrusions

Throughout the record instances of increased near-surface temperature occurred for shorter time periods (e.g in the middle of February and in the middle of March in 2002 as shown in Figure 2.5). The heat fluxes are directed from the ocean to the atmosphere during winter in the Greenland Sea and the anomalies reached too deep in the water column to originate at the surface. Hence, this increase in temperature must stem from water masses advected past the moorings (Latarius and Quadfasel, 2010). To restrict the analysis to the atmosphere's impact on the mixed-layer evolution, all profiles with such patches of warm water near the surface were removed.

Figure 2.5 shows the evolution of the heat content in the upper 300 m. The heat content H was calculated as

$$H = \rho c_p \int_{300m}^{Surface} T(z)dz \tag{2.1}$$

where ρ is the average density in the upper 300 m, c_p = 3850 J/kgK is the specific heat capacity of sea water, and T is the depth-dependent conservative temperature. As expected, the incidents with increased temperature coincide with periods of increased heat content in the upper 300 m. By manually inspection of the heat content time series from each winter we identified the events of warm intrusions as periods when the heat content increased. Within these periods, all profiles were removed until the heat content returned to the same level as prior to the intrusion. Profiles that were removed from the data set in winter 2001/2002 are indicated in gray in Figure 2.5.

In addition to removing the profiles substantially affected by advection, profiles where the mixed layer did not extend to the top of the mooring were also removed from the data set. Consequently, the data coverage was significantly reduced. From the original 928 profiles acquired during winter (Nov-Apr) throughout the 1999-2009 deployment period, only 453 profiles remained. Of these, only 360 had a mixed layer extending deep enough to be detected by the moorings.

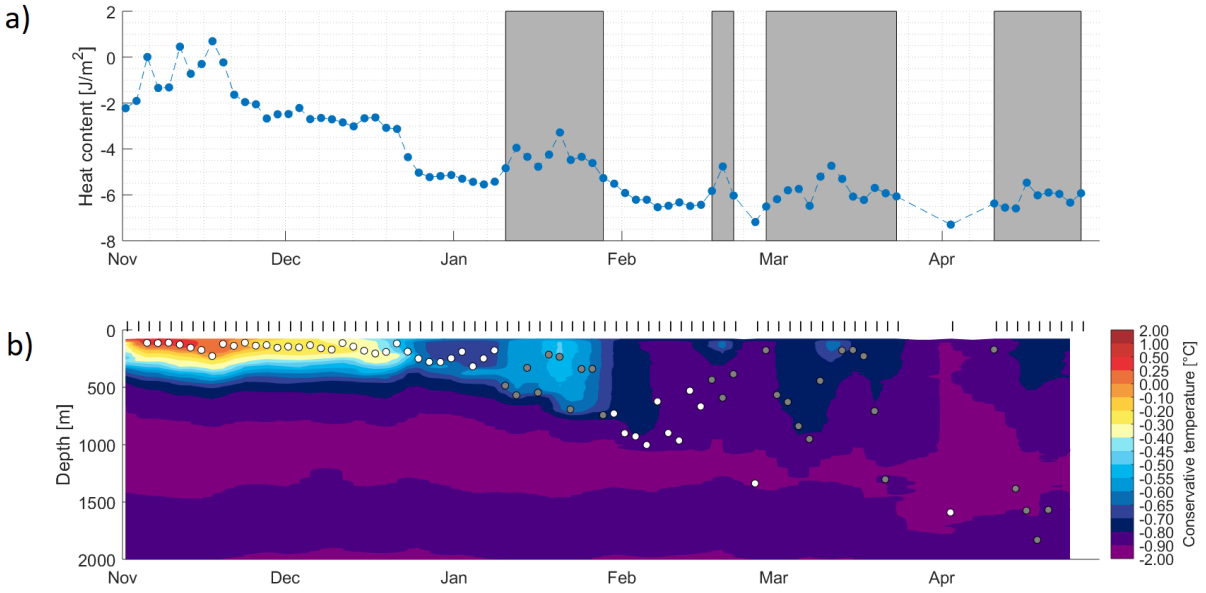

Figure 2.5: Evolution of heat content in the upper 300 m (a) and conservative temperature (b) for winter 2001/2002. The black bars at the top of panel (b) mark when profiles were obtained. Time periods when profiles were removed are shaded gray in (a). Mixed-layer depths are marked by white dots (gray for profiles that were removed).

2.5 Atmospheric data

The atmospheric data were obtained from the ERA-Interim reanalysis product, which is produced by the European Centre for Medium-Range Weather Forecasts (Dee et al., 2011). The reanalysis has a spatial resolution of 1° and covers the period from 1979 to present. Mean values from a box enclosing all three moorings were used (Figure 2.6). The box extends from 74 to 76 °N and from 2 to 5 °W. The variables used were sea ice concentration, surface skin temperature, potential temperature at 900 hPa, sensible and latent heat fluxes, radiative heat fluxes, wind stress, precipitation, and evaporation. The data cover the time period between January 1999 and December 2009 at six-hour intervals. Even though both turbulent and longwave radiation heat fluxes contribute to the total surface heat loss the mean net surface radiative flux varied little from year to year and the variability in turbulent heat flux accounts for most of the variability in total surface heat loss.

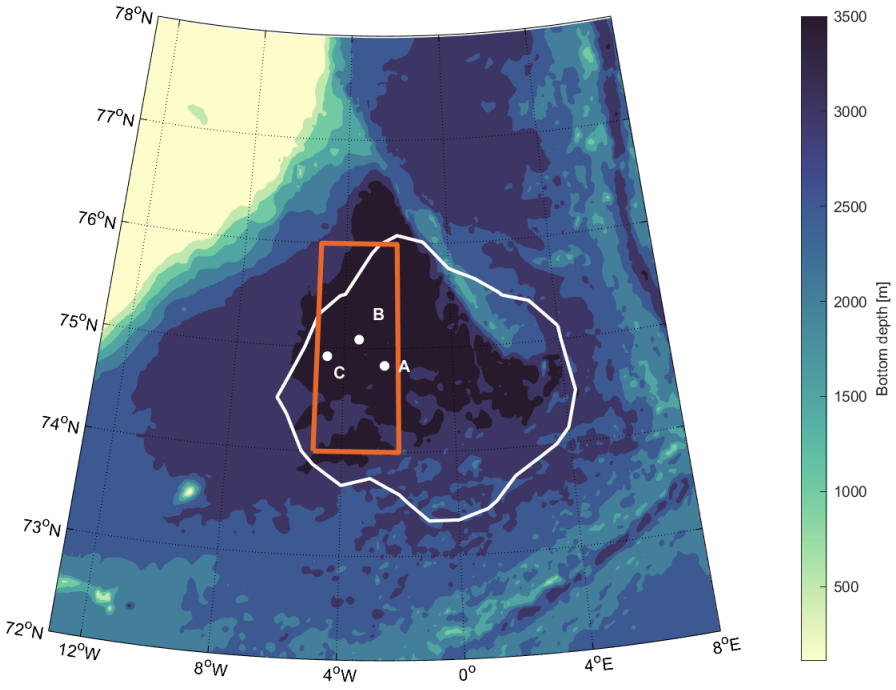

Figure 2.6: Map showing the box from where ERA-Interim data were extracted in orange. Mooring locations are marked by white dots and the outline of the Greenland Sea Gyre is shown in white.

2.6 Cold air outbreaks

Cold air outbreaks are characterized by a positive CAO-index (Section 1.5). In this study the index was defined as the difference $\theta_{SKT} - \theta_{900hPa}$, following Papritz and Sodemann (2018). θ_{SKT} is the surface skin temperature and θ_{900hPa} is the potential temperature at 900 hPa. Moderate to very strong cold air outbreaks are most important for dense water formation in the western Nordic Seas (Papritz and Spengler, 2017). Consequently, only CAOs with an index of 4K or higher were considered.

The CAOs were identified based on the CAO-indices as follows. The peak of the first event was defined as the highest ranked CAO-index. Every neighboring data point higher than 4K was then assigned to the event. The start and end of the event were set to the first and last data points where the CAO-index was higher than 4K. The next event was then identified following the same procedure, but without considering the data points that were attributed to the first event. In the end all events with peak values higher than 4K were identified, and all data points with a CAO-index higher than 4K were assigned to a particular event. Following Papritz and Spengler (2017), each event was identified as either moderate, strong, or very strong. The classification of each event was decided by its peak value. An example of CAO-indices through spring 2001 and the distribution of identified CAO events can be seen in Fig. 2.7.

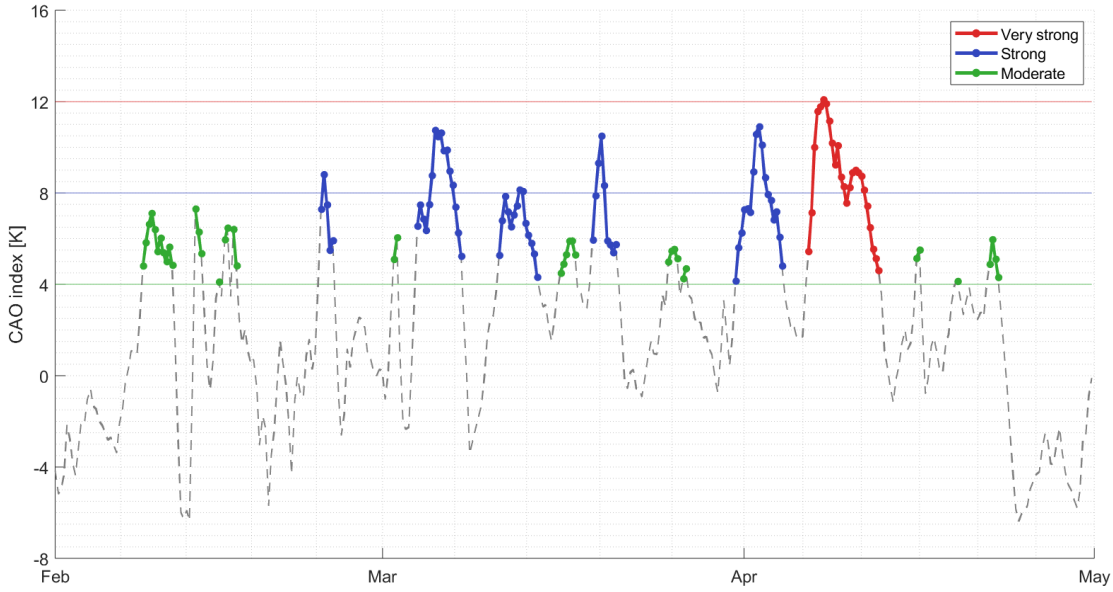

Figure 2.7: CAO-index through spring 2001. CAO events are marked in red (very strong), blue (strong), and green (moderate). The horizontal lines indicate the lower limits of each intensity class.

2.7 One-dimensional mixed-layer model

A one-dimensional mixed-layer model was employed in order to investigate the effects of atmospheric forcing and stratification on the mixed-layer evolution. The model was initially developed by Price et al. (1986) and is known as the Price-Weller-Pinkel (PWP) model. The model used in this study is a modified version of the PWP model. Moore et al. (2015) modified the model to include lateral advection of heat and Brakstad et al. (2019) further modified the model to also include lateral advection of salt and the production of sea ice. As atmospheric forcing the six-hourly ERA-Interim heat, freshwater, and momentum fluxes were applied (Section 2.5). The model was set up with a vertical resolution of 2 m and a time step of 6 hours.

At the beginning of each time step atmospheric heat and freshwater fluxes were imposed at the surface of the initial profile. Then vertical mixing and deepening of the mixed layer occurred until static stability was satisfied such that

$$\frac{\partial \rho}{\partial z} \geq 0 \tag{2.2}$$

where ρ and z are water density and depth, respectively. This vertical mixing simulates the convection driven by buoyancy loss at the surface. After static stability was achieved, wind stress induced momentum was added and the mixed layer was further adjusted by constraining the bulk R_b and gradient R_g Richardson numbers. To simulate mixed-layer entrainment the mixed layer entrained successively deeper levels until

$$R_b = \frac{g\Delta\rho h}{\rho_0(\Delta V)^2} \geq 0.6 \tag{2.3}$$

where h is the mixed-layer depth, V is the wind driven velocity, g is the gravitational acceleration, and $\rho_0 = 1024 kgm^{-3}$ is the reference density. In the case of shear flow instability, further deepening of the mixed layer took place until

$$R_g = \frac{g\frac{\partial\rho}{\partial z}}{\rho_0(\frac{\partial V}{\partial z})^2} \geq 0.25 \tag{2.4}$$

Shear flow instability is likely to occur over sharp density gradients typically found at the base of the mixed layer. In the Greenland Sea, the convection driven by buoyancy loss dominates the mixed-layer evolution (Brakstad et al., 2019).

Lateral fluxes of heat and salt from the surrounding water masses are also important for the structure of the water column in the Greenland Sea (e.g. Latarius and Quadfasel, 2010). Moore et al. (2015) and Brakstad et al. (2019) parameterized the advection of heat and salt, respectively, into the gyre by adding a fixed amount of heat and salt to the upper 1000 m of the water column at each time step. By balancing the annual-mean heat and freshwater budgets for the upper 1500 m of the Greenland Sea Gyre from 1986 to 2016, Brakstad et al. (2019) estimated the lateral heat input to be 61 W/m^2 and the freshwater removal to 4.5 mm/month. The same heat and freshwater fluxes were used in this study. The depth distribution of heat and freshwater fluxes were adjusted to reflect the hydrographic differences across the gyre boundary (Moore et al., 2015; Brakstad et al., 2019). An example of temperature and salt advection depth distributions to a profile with a 500 m deep mixed layer are shown in Figure 2.8. In the upper half of the mixed layer a constant temperature increase was added. Below this an exponentially decreasing amount of heat was added down to 1000 m. Salt, on the other hand, was removed in the upper half of the mixed layer to account for the input of fresh PSW. Deeper in the water column salt was added since the surrounding water masses are more saline than the gyre itself.

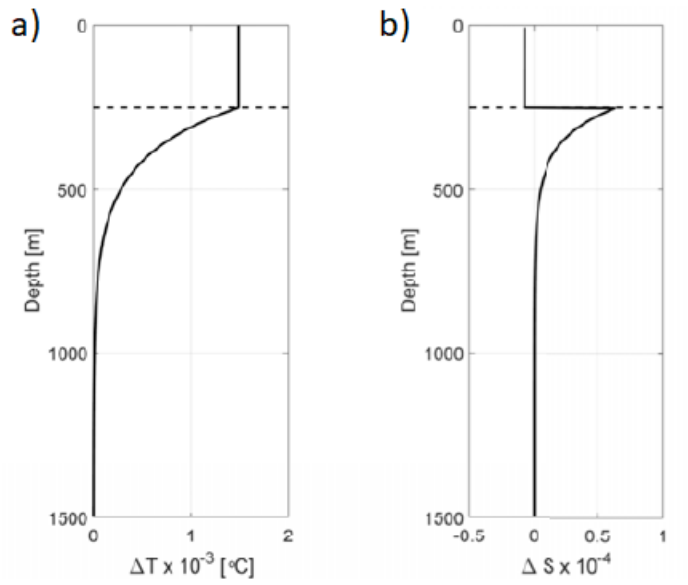

Figure 2.8: Example of depth distributions of lateral advection of heat (a) and salt (b) as parameterized in the model for a 500 m deep mixed layer. The black dashed lines mark the depth of the mixed layer divided by 2. (Figure B1 from Brakstad et al., 2019).

Chapter 3

Results

3.1 Hydrographic properties

By combining data from all three moorings (Section 2.3), the data set covered most of the time period between 1999 and 2009 (Figure 3.1). Only three winters were not covered. Throughout the decade the entire water column became warmer and more saline. In the upper 2000 m this development agrees well with both Lauvset et al. (2018) and Brakstad et al. (2019) who documented a warming and salinification in this depth range between 1986 and 2016. Lauvset et al. (2018) attributed this development to the increased temperature and salinity of the AW entering the Nordic Seas during the same time period. Currents carrying Atlantic-origin water is found both to the east and to the west of the Greenland Sea Gyre (Figure 1.1), and the warm and saline AW enters the gyre by eddy fluxes between 50 and 1500 m (Latarius and Quadfasel, 2016). Changes in the properties of the AW inflow hence affect the upper part of the water column in the Greenland Sea Gyre.

However, also the deepest part of the water column warmed throughout the deployment period (Figure 3.1a). This part of the water column consists of GSDW that has not been ventilated since deep-reaching convection ceased in the early 1980s (Section 1.4). After GSDW was isolated from the surface it could only be modified by horizontal exchange with deep waters from the Arctic Ocean through Fram Strait (Østerhus and Gammelsrød, 1999). Bottom waters from the Arctic Ocean are warmer and more saline than GSDW and leads to a warming and salinification.

In addition to the general warming and salinification, the upper 500 m of the water column were mainly dominated by the seasonal cycle, both in temperature and salinity (Figure 3.1). Between 500 and 2000 m the properties of the water column were affected by local convection each winter. The isopycnal $\sigma_\theta = 28.05$ kgm^{-3} was ventilated every winter, while during the last two winters (2007/2008 and 2008/2009) also the $\sigma_\theta = 28.06$ kgm^{-3} outcropped. The densest portion of the DSOW, which is transported towards the GSR in the NIJ, is denser than $\sigma_\theta = 28.03$ kgm^{-3}. As discussed in Section 1.3.1, dense water produced by wintertime convection in the Iceland Sea is hardly dense enough to contribute to this portion of the overflow. With mixed-layer densities exceeding $\sigma_\theta = 28.05$ kgm^{-3} each winter, convection in the Greenland Sea produced water masses

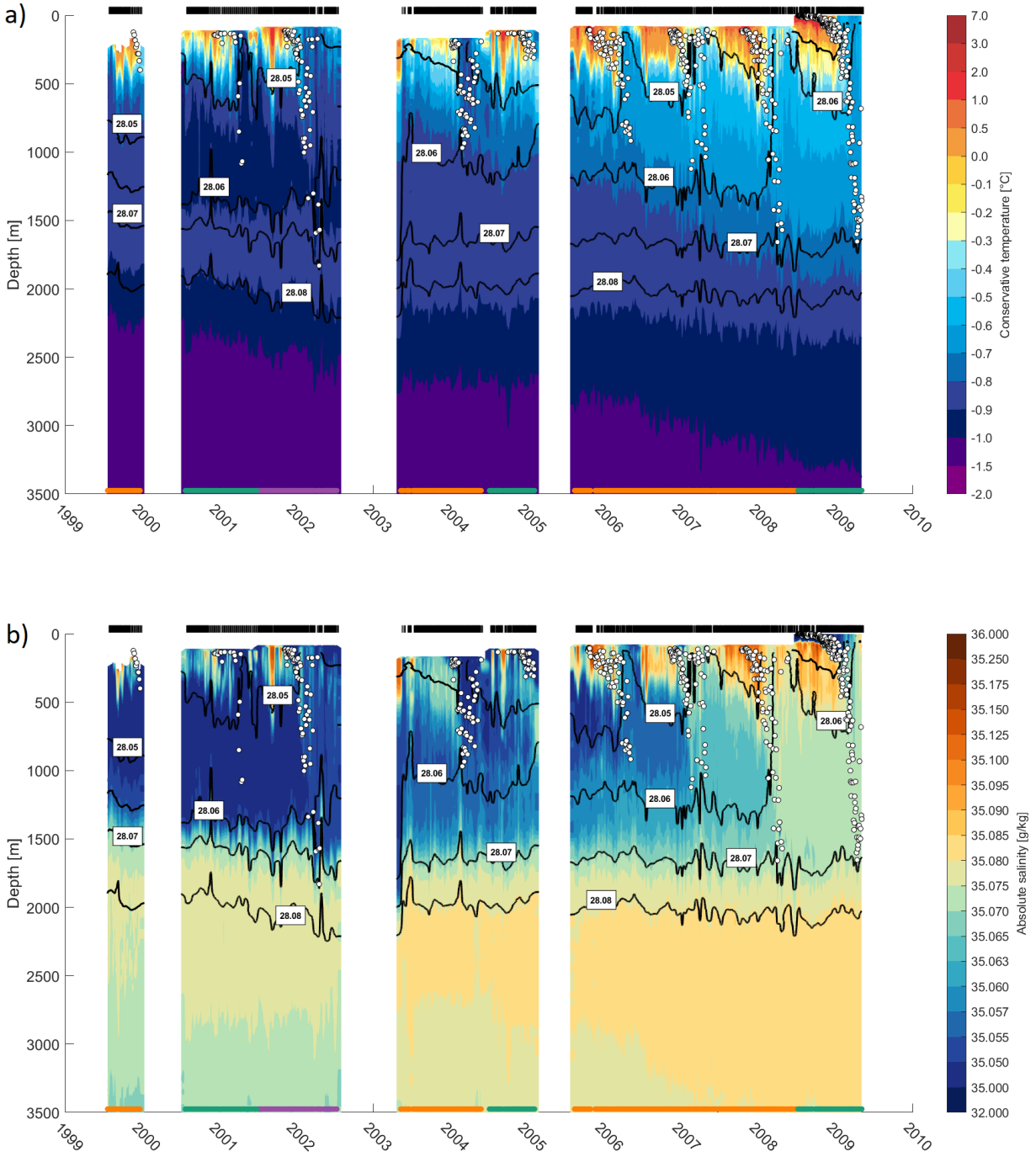

Figure 3.1: Conservative temperature (a) and absolute salinity (b) in the Greenland Sea Gyre from 1999 to 2009. Black lines show potential density contours. Mixed-layer depths are marked by white dots. The colors at the bottom of each figure indicate which mooring the data originate from (**mooring A**, **mooring B**, or **mooring C**). The black bars at the top of the figures mark when profiles were obtained.

sufficiently dense to contribute to the densest part of the DSOW.

The stratification of the water column is illustrated by the buoyancy frequency (Equation 1.1) in Figure 3.2. The part of the water column was characterized by a clear seasonal cycle with strong

stratification during summer due to radiative heating at the surface. During winter convection eroded the stratification. Between 500 and 2000 m the interannual variability in water column stability was large. Winters when deep convection occurred (such as 2001/2002 and 2007/2008) were clearly followed by summers where the water column was weakly stratified at intermediate depths. The relation between convection depth and water column stratification the consecutive summer was in particular evident in the stepwise increase of convection depth and concurrent decrease in stratification between 2006 and 2009. Prior to the winter 2005/2006 the water column was strongly stratified. During winter 2005/2006 the convection eroded the upper part of the stable water column and weakened the stratification down to approximately 1000 m. Convection the next winters eroded the stratification even further. There was clearly a relation between maximum mixed-layer depths each winter and the stratification of the water column the following summer.

Deep convection decreases the vertical density gradient and weakens the water column stratification. Ronski and Budéus (2005) used, amongst other criteria, the change in water column stratification to estimate depth of wintertime convection by comparing profiles from the Greenland Sea from two subsequent summers. Even though we have no measurements from winter 1999/2000, a trace of convection to about 1300 m can be inferred from the weakly stratified intermediate layer that appears in summer 2000. This pronounced decrease in buoyancy frequency from fall 1999 to summer 2000 was caused by convective mixing in winter 1999/2000.

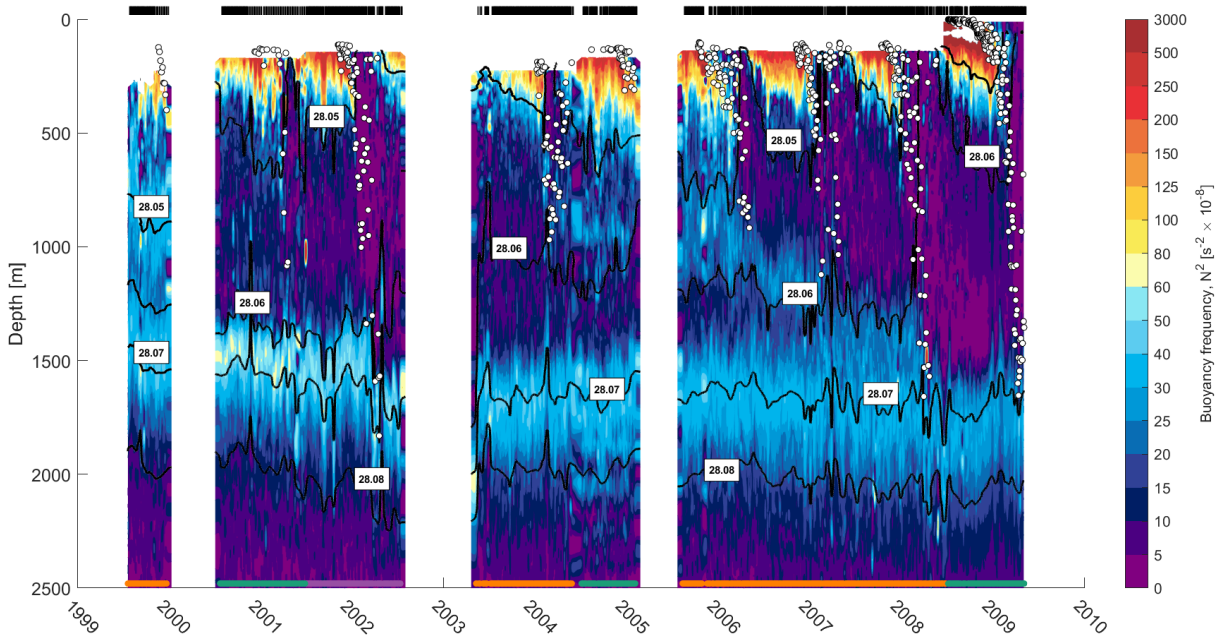

Figure 3.2: Buoyancy frequency in the Greenland Sea Gyre from 1999 to 2009. Black lines show potential density contours. Mixed-layer depths are marked by white dots. The colors at the bottom of each figure indicate which mooring the data originate from (**mooring A**, **mooring B**, or **mooring C**). The black bars at the top of the figures mark when profiles were obtained.

The intermediate temperature maximum around 1500 m before 2002 (Figure 3.1a) coincided

with a strong stability maximum (Figure 3.2). These maxima developed around 500 m in the early 1990s, separating the GSAIW from the deeper GSDW (e.g. Budéus et al., 1998; Karstensen et al., 2005, see also Section 1.4). Since then the maxima have descended gradually as the overlying GSAIW has been renewed through convection while the GSDW has remained isolated from ventilation. Even though the temperature maximum disappeared after 2002 (Figure 3.1a), the stability maximum has remained stable around 1500 m (Figure 3.2).

Another pronounced, intermediate layer of high stratification was also evident between 2004 and 2008 (also noted by Brakstad et al., 2019). After its inception at around 1000 m in 2004 it gradually descended concurrently with an increasing convection depth each winter until 2008 when it reached 1500 m and disappeared. Each winter deep convection eroded the stability maximum, increased the volume of weakly stratified water and deepened the depth of the stability maximum.

3.2 Interannual variability in convection depth

The winters with weaker atmospheric forcing than the overall mean generally had relatively shallow mixed-layers (not exceeding 1000 m; Figure 3.3). Deeper convection were observed when the winter mean turbulent heat flux was higher than the mean. However, the final convection depth each winter and the winter mean heat loss were not lineraly related. The stratification of the water column at the beginning of the winter also affects the depth of convection (Lauvset et al., 2018; Brakstad et al., 2019).

As a measure of fall stratification the mean buoyancy frequency between 200 and 1500 m depth (Equation 1.1) was calculated from October and November profiles. Mean fall stratification anomaly is indicated by color in Figure 3.3. The magnitude of the stratification below 200 m is insignificant if the mixed layer does not become sufficiently dense to erode the near-surface stability maximum that developed through the preceding summer. All winters occupied by the moored profilers had convective mixing well below this depth (see also Section 3.4). For the winters with weak atmospheric forcing (2005/2006 and 2003/2004) the fall stratification below 200 m largely did not affect the resulting convection depth. While the stratification was anomalously weak in fall 2003, the upper 1500 m were anomalously strongly stratified in fall 2005. Nevertheless, none of these winters had mixed layers exceeding 1000 m depth. Most of the total heat loss through winter was used to erode the near-surface stratification and the atmospheric forcing was too weak for convection to penetrate deeper.

During winters with stronger atmospheric forcing the fall stratification was more important for the final convection depth. Even though winters 2006/2007 and 2007/2008 were exposed to approximately the same amount of turbulent heat loss to the atmosphere ($\sim$135 W/m^2), the maximum observed mixed-layer depth differed by almost 600 m. The fall stratification below 200 m, which was anomalously strong in 2006/2007 and anomalously weak in 2007/2008, was the main reason for the discrepancy. While the atmospheric forcing was sufficiently strong to erode the near-surface

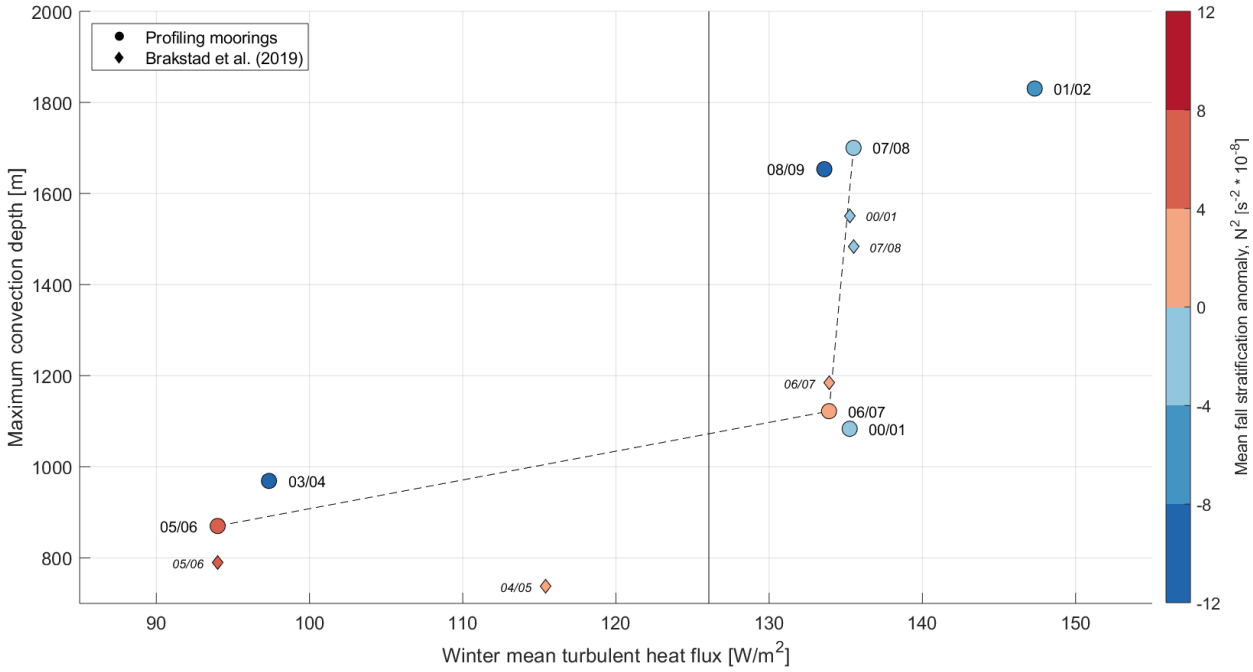

Figure 3.3: Annual maximum mixed-layer depth between 1999 and 2009 as a function of winter(Nov-Apr) mean turbulent heat flux. Mean buoyancy frequency anomaly for the water column between 200 and 1500 m the preceding fall (Oct-Nov) is shown in color. The average buoyancy frequency over this depth range through the entire period was 2.7 $\times$ 10^{-7} s^{-2}. The vertical black line marks the winter mean turbulent heat flux through the period, which was 126 W/m^2. The evolution from 2005/2006 to 2007/2008 is illustrated by the black, dashed line. Annual maximum mixed-layer depths in the Greenland Sea Gyre determined by Brakstad et al. (2019) are indicated with diamonds.

stratification both years, the stronger stratification below 200 m in 2006/2007 inhibited convection from reaching the same depths as the year after. The winter 2000/2001, when the mean turbulent heat flux was also approximately 135 W/m^2, had anomalously weak fall stratification. Yet convection did not reach deeper than 1000 m. This was a result of winter sea ice which covered the mooring locations through most of January and February. The sea ice isolated the sea surface and prevented heat loss to the atmosphere (Section 3.3). Brakstad et al. (2019) investigated profiles collected within the entire Greenland Sea Gyre (annual maximum convection depth each winter indicated by diamonds in Figure 3.3) and found a maximum mixed-layer depth of 1550 m in 2000/2001, which agrees better with the pattern from the other winters. Apart from winter 2000/2001 with substantial ice cover, our observed mixed-layer depths are in good agreement wit the results from Brakstad et al. (2019).

The stepwise increase in convection depth from 2005 to 2008 described in Section 3.1 is denoted by a black dashed line in Figure 3.3. The convection, which reached deeper each successive winter, weakened the stratification of the water column and preconditioned the region for deeper convection the subsequent winter. This gradual decrease in water column stability resulted in the weakest fall stratification observed throughout the record in 2008/2009. However, the gradual in-

crease in convection depth did not continue from 2007/2008 to 2008/2009, even though the latter experienced a similar amount of heat loss. The convection these two winters (both to about 1700 m deep), reached the stratification maximum that separates the GSAIW from the deeper GSDW (Figure 3.2). Even though the fall stratification in 2008 was the weakest observed from the entire period, and the atmospheric forcing was relatively strong, the heat loss was not sufficient to erode through the deep stability maximum.

3.3 Mixed-layer depth evolution

After profiles that were substantially affected by advection were removed (Section 2.4), the deepening of the mixed layer each winter was evident (Figure 3.4). The 30-day running means, in particular, illustrate well how the mixed layer evolved through the winter. There were clear interannual variations in how deep the mixed layer became each winter. More than 1000 m separated the shallowest (2005/2006) and deepest (2001/2002) convection depths. Nevertheless, the mixed-layer evolution each winter had a similar pattern, which can be separated into three distinct phases. The mixed-layer depth was shallow and changed little throughout the first phase in early winter, before it rapidly deepened during the second phase. In the third phase, at the end of winter, the rapid deepening ceased and the mixed-layer depth stabilized.

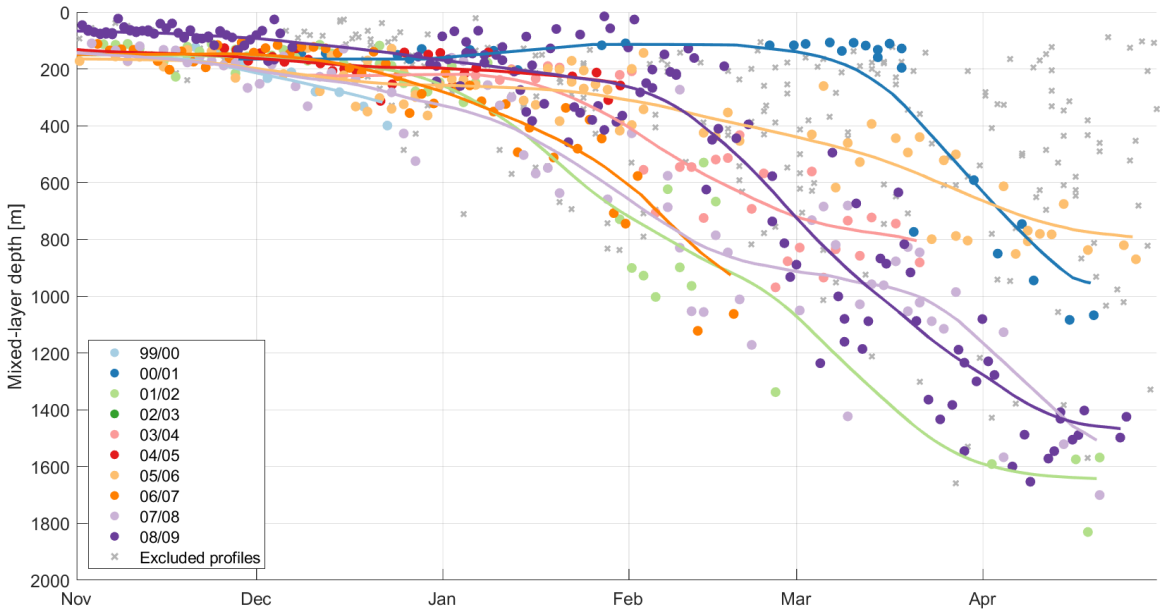

Figure 3.4: Wintertime evolution of mixed-layer depth. Each color represents different winters. The lines are 30-day running means. The gray crosses represent mixed-layer depths that were excluded from the analysis (Section 2.4).

Total monthly changes of mixed-layer depth and temperature were determined (Figure 3.5). Within each month, a linear regression line for all data points was calculated, and the monthly

change was determined as the difference between the value of the regression line at the beginning and at the end of the month. Some months had large variability in mixed-layer depth changes between the winters, but the mean values showed a similar signal as the smoothed lines in Figure 3.4. The mixed-layer depth changed little early in the winter (i.e. November and December), while the maximum deepening rate was found in February. Later in winter (March and April) the mixed layer deepened more slowly again (Figure 3.5b). The mixed-layer temperature changed most during months when the mixed-layer depth changed little (Figure 3.5b). Most of the temperature decrease occurred early in the winter (November and December), while later in the winter the mixed-layer temperature stayed relatively unchanged. Summing the monthly mean changes over the whole winter gives a total cooling of 2.6°C and a deepening of 1600 m for the average mixed layer. These numbers agree well with the typical observed changes (Figure 3.4 for mixed-layer depth, not shown for temperature).

For each winter the transitions between the three phases were identified based on the inflection points of the running mean of the time series. The beginning of phase 2 was set to the first point where the second derivative had a minimum after mid-December, i.e. the first negative inflection point. The transition from phase 2 to phase 3 was defined as the last point where the second derivative had a maximum, so long as it occurred after mid-March, i.e. the last positive inflection point. For all winters very few profiles were available from phase 3. Hence, only phase 1 and phase 2 are considered in the analysis. The transition points between phases 1 and 2 are marked by stars in Figure 3.6, which shows the time series normalized by each year's maximum convection depth.

The transition from phase 1 to phase 2 generally occurred between late December and early February. One exception was the winter of 2000/2001 when phase 2 started 11. March. Unlike the other years the mooring locations were covered by sea ice through most of January and February that winter (not shown). The ice cover insulated the sea surface from atmospheric heat loss and was accompanied by a layer of very cold and fresh water which kept the mixed layer shallow. When the ice edge retreated in March the water column was exposed to the atmosphere and phase 2 of the convection process began shortly thereafter. While the moorings were covered by sea ice, the mixed layer was mostly too shallow to be detected (see the sparse sampling between January and February in Figure 3.6). These under-ice profiles that are not directly exposed to the atmosphere are not included in the following analysis.

3.4 Short-term variability in mixed-layer properties

Changes in mixed-layer depth and temperature from profile to profile were calculated at each separate mooring location to study the short-term response of the mixed layer to various atmospheric forcing. To ensure that the evolution primarily was due to atmospheric forcing, only changes between profiles acquired less than five days apart were included and the profile-to-profile change was divided by the time span between the profiles to get daily rate of change. The changes in mixed-layer properties were classified by phase and turbulent heat flux Figure 3.7. Within each

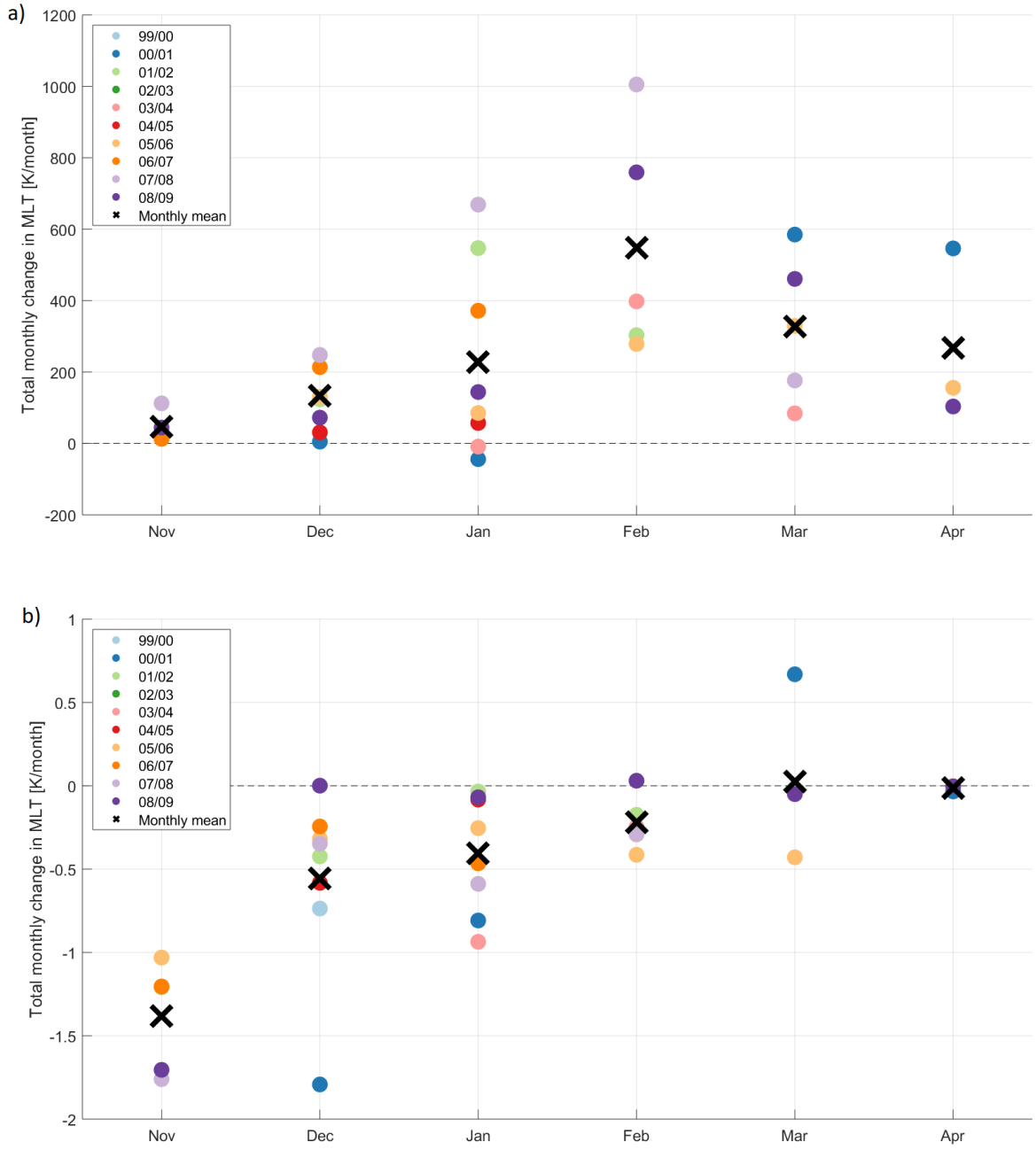

Figure 3.5: Monthly change in mixed-layer depth (a) and temperature (b) each winter. Each color represents different winters, corresponding to the colors in Figure 3.4. The mean values for each month are marked with black crosses.

phase and range of turbulent heat flux, outliers that differed more than three median absolute deviations from the median were removed.

In phase 1 the mixed-layer depth increased slowly, even when the atmospheric forcing was strong (Figure 3.7a). The median increase did not exceed 8 m per day, regardless of the magnitude of the heat loss. In phase 2 the mixed-layer depth growth rate clearly increased with intensifying heat fluxes. For the strongest atmospheric forcing the mixed-layer depth increased by up to 180 m

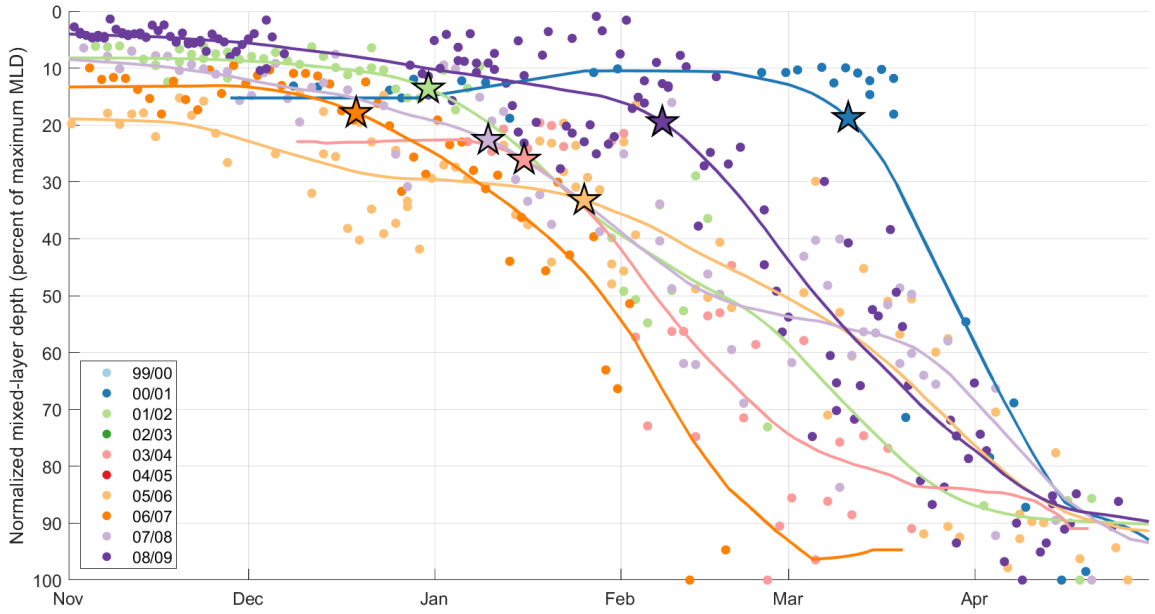

Figure 3.6: Wintertime evolution of mixed-layer depth normalized by the maximum convection depth each winter. Each color represents different winters. The lines are 30-day running means. The stars indicate the transition between the first and the second phase of convection (see text for details).

per day. During periods of weak heat fluxes the phase 2 mixed-layer depth shoaled. In addition to being cooled by the atmosphere the water column in the Greenland Sea Gyre is constantly affected by a substantial positive lateral heat flux from surrounding Atlantic-origin water (e.g. Latarius and Quadfasel, 2016). The negative change in mixed-layer depth for heat fluxes in the range 0-99 W/m^2 indicate that to deepen or maintain mixed-layer depth stronger atmospheric forcing was required. During periods with weak heat fluxes the development of the water column was dominated by lateral fluxes which led to a temporary restratification and shallower mixed layers. Even though clear patches of warm water near the surface were removed (Section 2.4), constant supply of warmer, ambient water masses at greater depths took place throughout the year and might have contributed to a shoaling of the mixed layers during periods of weak atmospheric forcing Figure 3.7.

For all but one winter the mean turbulent heat flux throughout phase 2 was higher than 130 W/m^2 (not shown). This implies that even though shorter time periods had weak atmospheric forcing when the mixed-layer depth decreased, the heat fluxes were generally strong enough to maintain or increase the depth of the mixed layer. The exception was winter 2003/2004 when the phase 2 mean turbulent heat flux was 84 W/m^2. Such weak atmospheric forcing was not able to compensate for the heating by lateral intrusions, and this winter was one of the winters with the shallowest convection (Figure 3.4).

While the greatest changes in mixed-layer depth occurred in the second phase, the mixed-layer temperature remained approximately unchanged (Figure 3.7b). The median values were approxi-

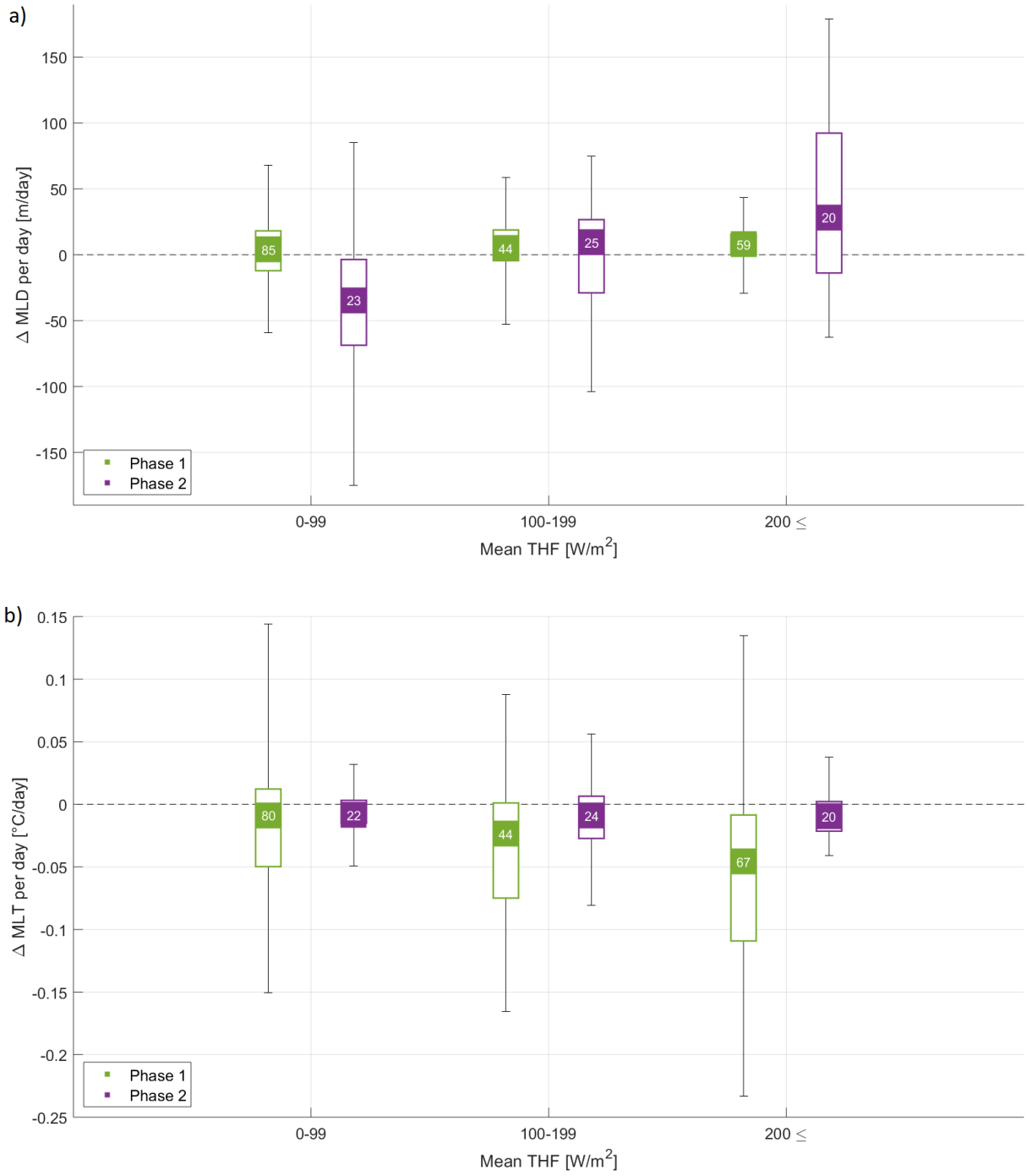

Figure 3.7: Daily change in mixed-layer depth (a) and temperature (b) calculated from profiles acquired less than five days apart. The values are grouped according to mean turbulent heat flux and the phase in which the change took place. The squares mark median values, while the lower and upper limits of the boxes indicate the 25th and 75th percentiles, respectively. The whiskers show maximum and minimum values after exclusion of outliers. Changes in phase 1 are shown in **green** and changes in phase 2 in **purple**. The number of data points available within each phase and heat flux range is indicated inside each box.

mately -0.009 °C per day regardless of the intensity of the turbulent heat flux and the variability was relatively small. During the first phase, on the other hand, changes in mixed-layer tempera-

ture were substantial, in particular for high heat fluxes. For the strongest atmospheric forcing the temperature decreased by up to 0.23°C per day.

In the beginning of winter, during the first phase of the mixed-layer evolution, the mixed layer was generally less than 200 m deep (Figure 3.4). The shallow mixed layers required less atmospheric forcing to cool the entire layer compared to the deeper mixed layers found in phase 2. Thus the changes in mixed-layer temperature were more pronounced in phase 1 than in phase 2. When the near-surface stratification was eventually eroded, the second phase commenced and the mixed layer deepened rapidly. Consequently the greatest changes in mixed-layer temperature were observed during phase 1, while the most pronounced changes in mixed-layer depth occurred in the second phase.

The daily change of heat content (Equation 2.1) in the active part of the water column was also calculated for each pair of profiles (Figure 3.8). The active part was defined as the depth between the surface and the deepest of the mixed layers from the two profiles. In both the first and the second phases, the heat content decreased more rapidly during periods with stronger atmospheric forcing. Because the heat content is derived from the depth-integrated temperature, both changes in temperature and depth of the mixed layer were taken into account. This means that the decreasing mixed-layer temperature in phase 1 and the increasing mixed-layer depth in phase 2 in total contributed to a decrease in heat content during both phases. The large variability indicates that processes other than heat loss to the atmosphere, such as lateral heat fluxes, are also important for the seasonal evolution of the mixed-layer.

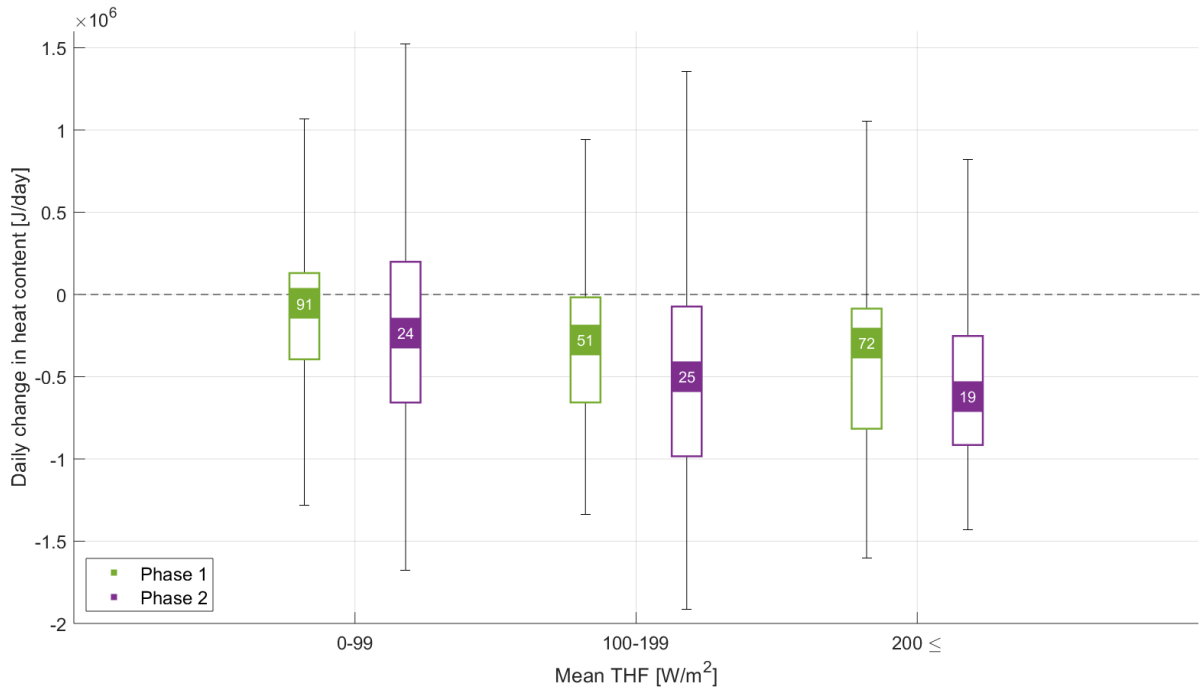

Figure 3.8: Daily change of heat content in the active part of the water column calculated from profiles acquired less than five days apart. The values are grouped according to mean turbulent heat flux and the phase in which the change took place. The squares mark median values. The lower and upper limits of the boxes mark the 25th and 75th percentile, respectively. The whiskers show maximum and minimum values after exclusion of outliers. Changes in phase 1 are shown in **green** and changes in phase 2 in **purple**. The number of data points available within each phase and heat flux range is indicated inside each box.

3.5 Contribution from cold air outbreaks

The 6-hourly mean turbulent heat flux generally increased with higher CAO-indices Figure 3.9. The regression line in Figure 3.9 was found by least square method and has a slope of 26 W/m^{2}K, indicating that as the CAO-index increased by 1K, the turbulent heat flux increased by 26 W/m^{2}K. The slope in Figure 3.9 is plotted against instantaneous CAO-indices, independent of whether the data points were part of a cold air outbreak event with stronger intensity. The method used to identify cold air outbreaks attributed many 6-hour periods of relatively low CAO-index to stronger events as the strength of the event was defined by it peak CAO-index value Section 2.6. Nevertheless, Figure 3.9 shows that such periods with CAO-index higher than 4K generally contributed greatly to the mean winter turbulent heat flux. For the highest cold air outbreak intensities, the turbulent heat fluxes were up to 660 W/m^2.

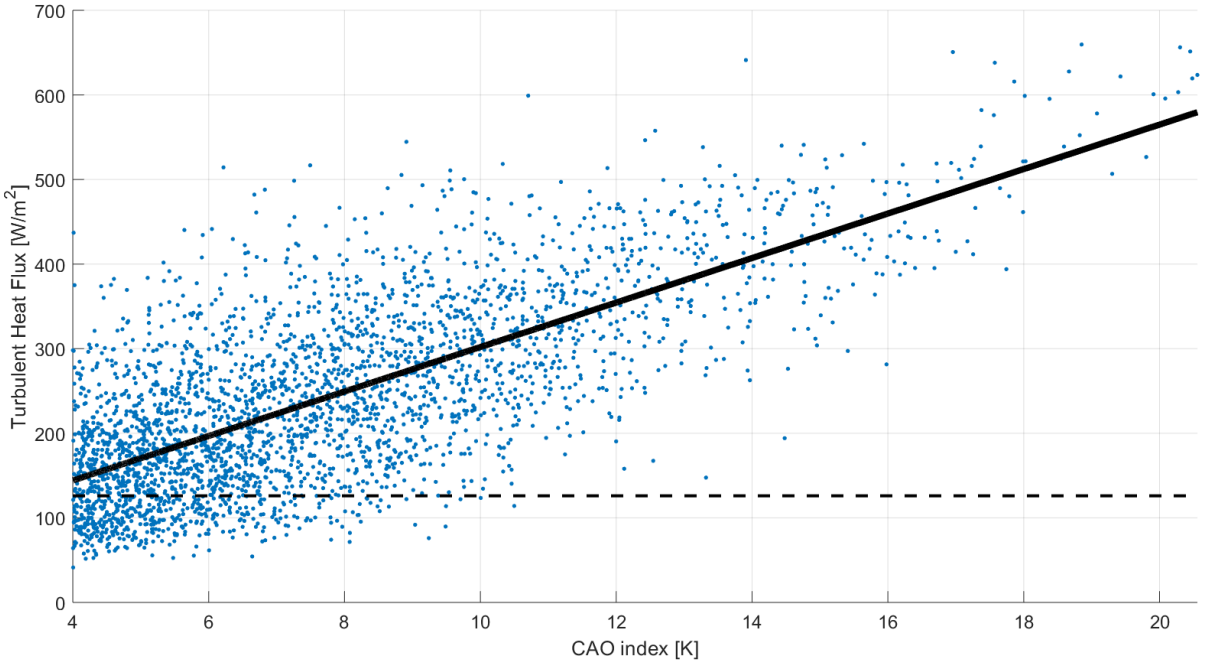

Figure 3.9: Turbulent heat flux plotted against CAO-index. Each point represents data from a six-hour interval between 1999 and 2009. The black line is the linear regression with a slope of 26 W/m^{2}K. The mean winter (Nov-Apr) turbulent heat flux through the whole period (126 W/m^2) is marked by the dashed, black line.

3.5.1 Interannual variability

Throughout the record cold air outbreaks accounted for 50-80 % of the total turbulent heat loss from the ocean to the atmosphere (Table 3.1). These numbers corroborate the results from Papritz and Spengler (2017) that cold air outbreaks are important for the turbulent heat loss in the Greenland Sea. Even during winter 2005/2006 when cold air outbreaks were present only during 18 % of the winter, the events were responsible for nearly 60 % of the total heat loss. However, that winter the mean turbulent heat flux was particularly low (94 W/m^2). In general, most of the heat loss from the ocean to the atmosphere each winter occurred during cold air outbreaks.

Table 3.1: Frequency of CAOs and their contribution to the total turbulent heat loss through each winter.

Winter (Nov-Apr)	Mean turbulent heat flux [W/m^2]	Frequency of CAOs	Contribution to total turbulent heat loss by CAOs
1999/2000	174	47 %	77 %
2000/2001	135	31 %	61 %
2001/2002	147	45 %	78 %
2002/2003	94	28 %	73 %
2003/2004	97	29 %	72 %
2004/2005	115	27 %	61 %
2005/2006	94	18 %	57 %
2006/2007	134	33 %	68 %
2007/2008	136	36 %	70 %
2008/2009	134	37 %	69 %

3.5.2 The role of cold air outbreaks on short-term variability in the mixed layer

To link the short-term variability in mixed-layer properties (Section 3.4) to the presence of CAOs, the profile-to-profile changes were grouped according to the strength of the CAO in which the change occurred (Figure 3.10). Changes when at least one of the profiles were acquired during a CAO event were grouped according to the intensity of the event. Since CAOs are characterized by strong atmospheric forcing, the results in Figure 3.10 resembled Figure 3.7 in many ways and the changes in mixed-layer properties seen during the strongest CAOs were the same changes as during high heat fluxes. The mixed-layer depth changed little during phase 1 for all classes of CAOs, while in phase 2 the mixed-layer depth deepened more rapidly during very strong events. The median value of mixed-layer depth changes during very strong events in the second phase was 28 m/day. The mixed-layer temperature, on the other hand, showed minor change during phase 2 and a clear increased cooling with stronger CAOs in phase 1.

Consequently, the strong and very strong CAOS that occurred early in winter stood for periods of strong atmospheric forcing that cooled the mixed layer and densified it sufficiently for phase 2 of the convection process to start. Later in winter the strongest CAOs led to a deepening of the mixed layer while the temperature stayed relatively unchanged. After the onset of phase 2, the mixed layer has reached below the near-surface stratification (Figure 3.2) to depths with significantly weaker stratification such that a minor reduction in temperature (and an associated small increase in density) were enough to deepen the mixed layer substantially. For the weakest CAOs some of the median changes in mixed-layer depth were negative (both in phase 1 and 2) and the median mixed-layer temperature changes were positive during phase 1. The reason for this was as discussed in Section 3.4 that lateral advection restratified the water column by supplying warm and saline water masses.

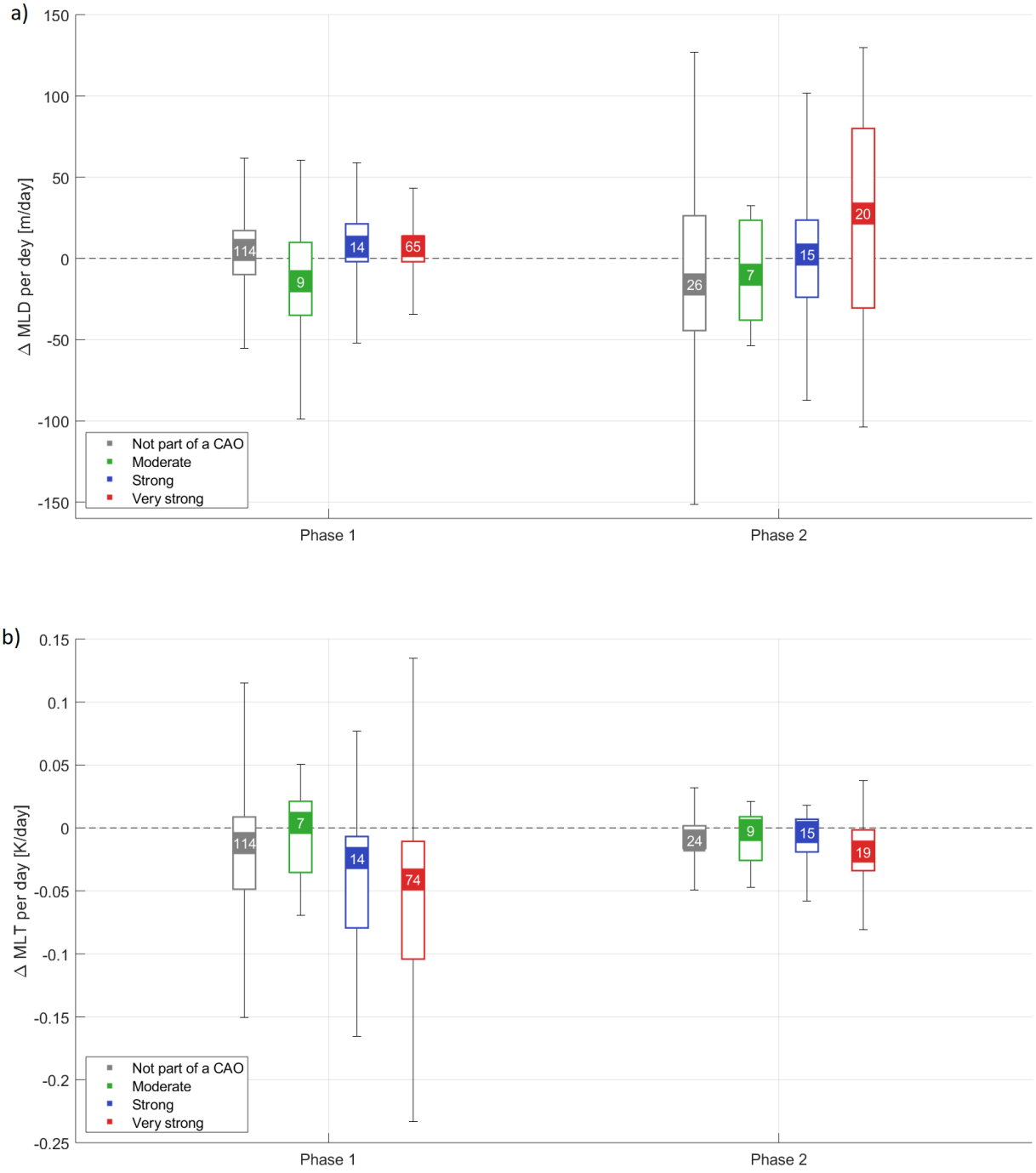

Figure 3.10: Daily change in mixed-layer depth (a) and temperature (b) calculated from profiles taken less than five days apart and grouped by phase. Changes when at least one of the profiles were acquired during a CAO event are grouped according to the intensity of the event (**moderate**, **strong**, or **very strong**). Changes where none of the profiles were part of a CAO are shown in grey. The squares mark median values. The lower and upper limits of the boxes mark the 25th and 75th percentile, respectively. The whiskers show maximum and minimum values after exclusion of outliers. The number of data points available within each phase and intensity class is indicated inside each box.

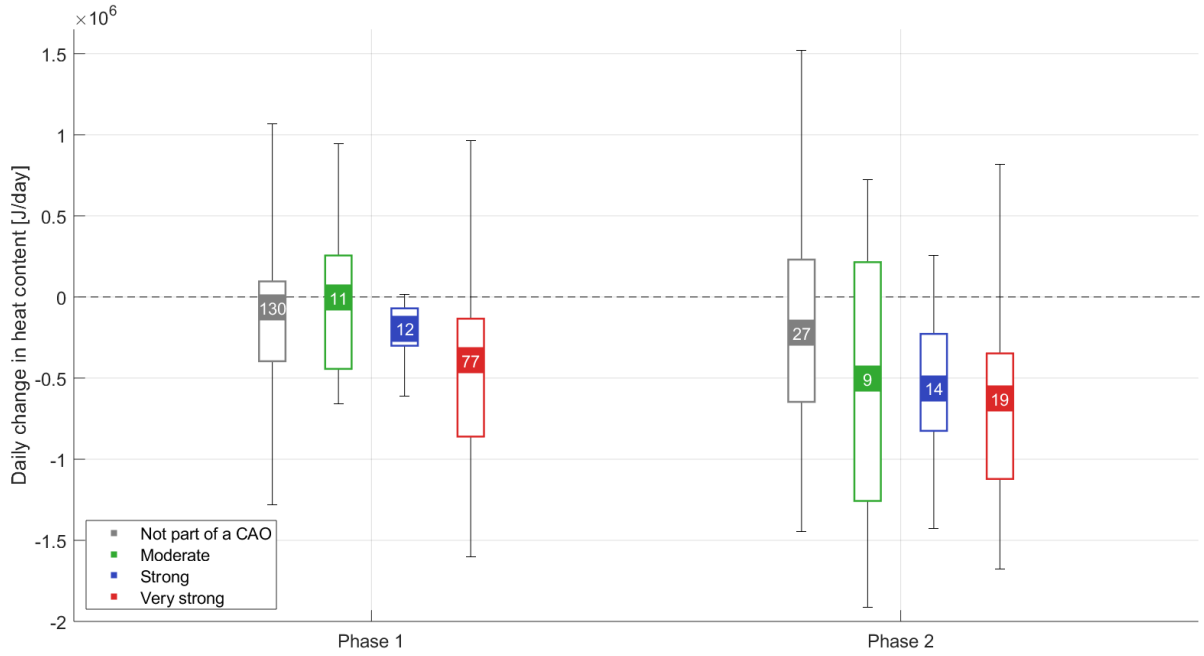

Figure 3.11: Daily change in heat content in the active part of the water column, calculated from profiles taken less than five days apart and grouped by phase. Changes when at least one of the profiles were acquired during a CAO event are grouped according to the intensity of the event (**moderate**, **strong**, or **very strong**). Changes where none of the profiles were part of a CAO are shown in grey. The squares mark median values. The lower and upper limits of the boxes mark the 25th and 75th percentile, respectively. The whiskers show maximum and minimum values after exclusion of outliers. The number of data points available within each phase and intensity class is indicated inside each box.

The change in heat content was higher during the strongest CAO events (Figure 3.11). This pattern was similar in both phases because the heat content takes changes both in temperature and depth into account. The strongest CAOs that took place in phase 1 led to a decrease in heat content by cooling the mixed layer (Figure 3.10b). In phase 2, the CAOs contributed to decreased heat content by increasing the depth of the mixed layer (Figure 3.10a).

3.6 Idealized simulations of mixed-layer depth evolution

To investigate the effects of atmospheric forcing and stratification on the mixed-layer depth evolution a one-dimensional mixed-layer model was employed (described in Section 2.7). The objective was to investigate whether the distribution of heat loss throughout the winter affects the resulting convection depth and to examine the magnitude of heat loss needed to re-ignite bottom-reaching convection. The mixed-layer evolution each winter was simulated and compared to observations. The model generally performed well and the simulated mixed-layer depths were in good agreement with the observations (examples from 2005/2006 and 2007/2008 are shown in Figure 3.14). The resulting end-of-winter convection depth was, however, consequently underestimated (shown for

2005/2006 and 2007/2008 in Figure 3.14). Most winters the underestimation was insignificant, but in 2001/2002 and 2008/2009 the error exceeded 500 m and the model did not satisfactorily reproduce the winter evolution.

As initial conditions the first profile each winter where the mixed layer was identified was used (Figure 3.12). Most winters the initial profile was from early November, but in winter 2003/2004 the mixed layer did not reach the mooring until January. Also in winter 2008/2009 a profile from January was used. Even though mixed layers were detected in early November by the shallow moored profile, the joint between the shallow and deep measurements made the profile discontinuous and not favorable as initial conditions. Instead, the profile from when the mixed layer consistently was detected by the deep moored profiler was used. For each winter the model was run from the time of the initial profile.

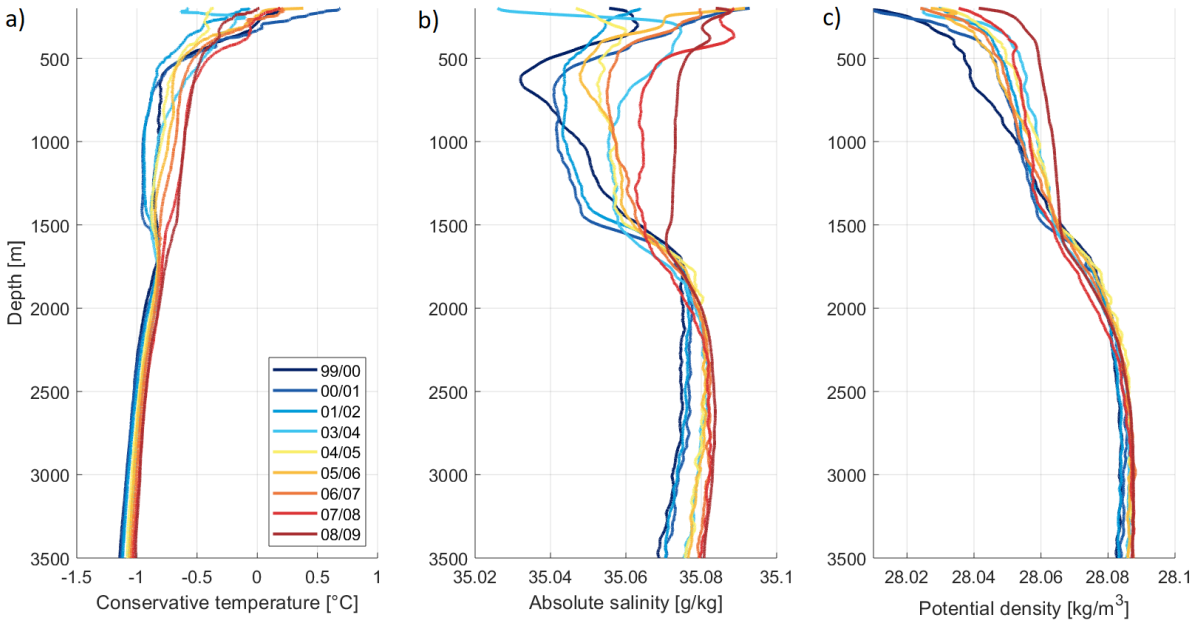

Figure 3.12: Conservative temperature (a), absolute salinity (b) and potential density (c) profiles used as initial conditions in the mixed-layer model. Each color represents different winters.

The warming and salinification of the water column (Section 3.1) can clearly be seen in the initial profiles, in particular at intermediate depths (Figure 3.12). In the corresponding profiles of buoyancy frequency (Figure 3.13) the stability maximum separating the GSAIW from the deeper GSDW was evident just below 1500 m in 1999. The maximum gradually descended and weakened throughout the deployment period and in 2008 it was situated around 1700 m. The intermediate stability maximum that was formed around 1000 m in 2004 (Section 3.1), and how it descended each year until 2008, is also visible in Figure 3.13.

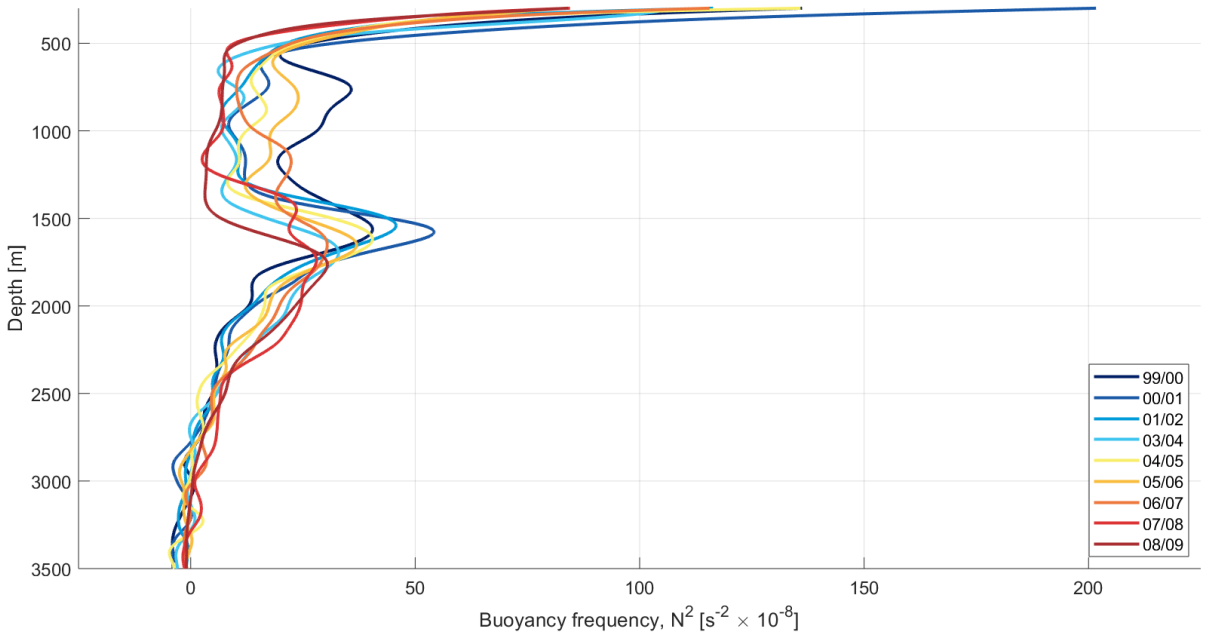

Figure 3.13: Buoyancy frequency for the profiles used as initial conditions in the mixed-layer model. Each color represents different winters.

3.6.1 Heat loss distribution

The importance of the wintertime heat loss distribution was studied by applying different idealized atmospheric forcing time series to the initial condition profiles. The results of the different simulations from 2005/2006 and 2007/2008 are shown in Figure 3.14. In addition to the actual forcing (noted as ERA-Interim in Figure 3.14) a time series where most of the heat loss was concentrated early in winter and one where most of the cooling occurred late in winter were considered. To simulate early heat loss an atmospheric forcing time series with a constant heat loss of 1.5 times the ERA-Interim mean during the first half of the winter and 0.5 times the mean during the last half was applied. The time series used to simulate late heat loss was constructed similarly with a constant heat loss of 0.5 times the ERA-Interim mean during the first half of the winter and 0.5 times the mean during the last half. In this way the mean heat loss from all time series was identical. A constant forcing equivalent to the mean of the actual forcing was also applied (not shown).

The simulated mixed layer evolution through winter differed when the heat loss was distributed differently. In particular the onset of phase 2 (the period in which most of the mixed-layer deepening occurs, see section Section 3.3) seemed to be strongly dependent on the heat flux distribution. While the mixed layer deepened steadily through the winter when the atmospheric forcing was constant, the simulations with early and late heat loss were both characterized by shorter time periods of rapid mixed-layer deepening. The start of phase 2 occurred early in winter when heat fluxes were strongest in fall and late in winter when most of the heat loss occurred after January.

For all winters, the simulated depth of convection reached deepest when the heat loss was concentrated in the first half of the winter (Figure 3.14). The upper part of the water column is continuously supplied with heat through lateral fluxes (Latarius and Quadfasel, 2016). In the simulations where the atmospheric forcing strengthened late in winter the surface layer had gained so much heat that more cooling was required to obtain the same convection depth as when the heat loss was concentrated at the beginning of the winter.

3.6.2 Forcing required for bottom-reaching convection

Below the stability maximum at 1500 m the water column stratification was very weak (Figure 3.2). Therefore, if convection had been sufficiently deep to penetrate the stability maximum, the mixed layer could probably easily have reached the bottom. To investigate the possibility of bottom-reaching convection, atmospheric forcing time series of different strength were applied to the initial profile from 2007/2008. To simulate atmospheric forcing of different strength multiples of the actual forcing time series from ERA-Interim were used.

The mixed-layer depth in 2007/2008 was among the deepest in the record (Figure 3.3), and the model accurately reproduced the convective evolution this winter. It would have been interesting to investigate the succeeding winter (2008/2009) as well, since the water column stratification in fall 2008 was the weakest throughout the record. This was, however, not possible because of the late initial profile and the distinct joint at 130 m that resulted from the merging of data from two separate moored profilers.

The simulated end-of-winter profiles with maximum convection depth are shown in Figure 3.15. The stability maximum was located between 1300 and 2200 m, where the density gradient was largest in the initial profile. For stronger atmospheric forcing convection eroded deeper into the stability maximum. When the model was ran with atmospheric forcing three times stronger than the actual forcing, the heat loss was large enough for the convection to exceed the depth of the stability maximum. The mixed layer then rapidly deepened all the way to the bottom. A three-fold increase in heat loss is, however, not realistic. The strongest winter mean heat flux between 1999 and 2009 occurred during winter 1999/2000. This winter the heat fluxes were 1.2 times stronger than in 2007/2008, which is not nearly enough to erode through the stability maximum.

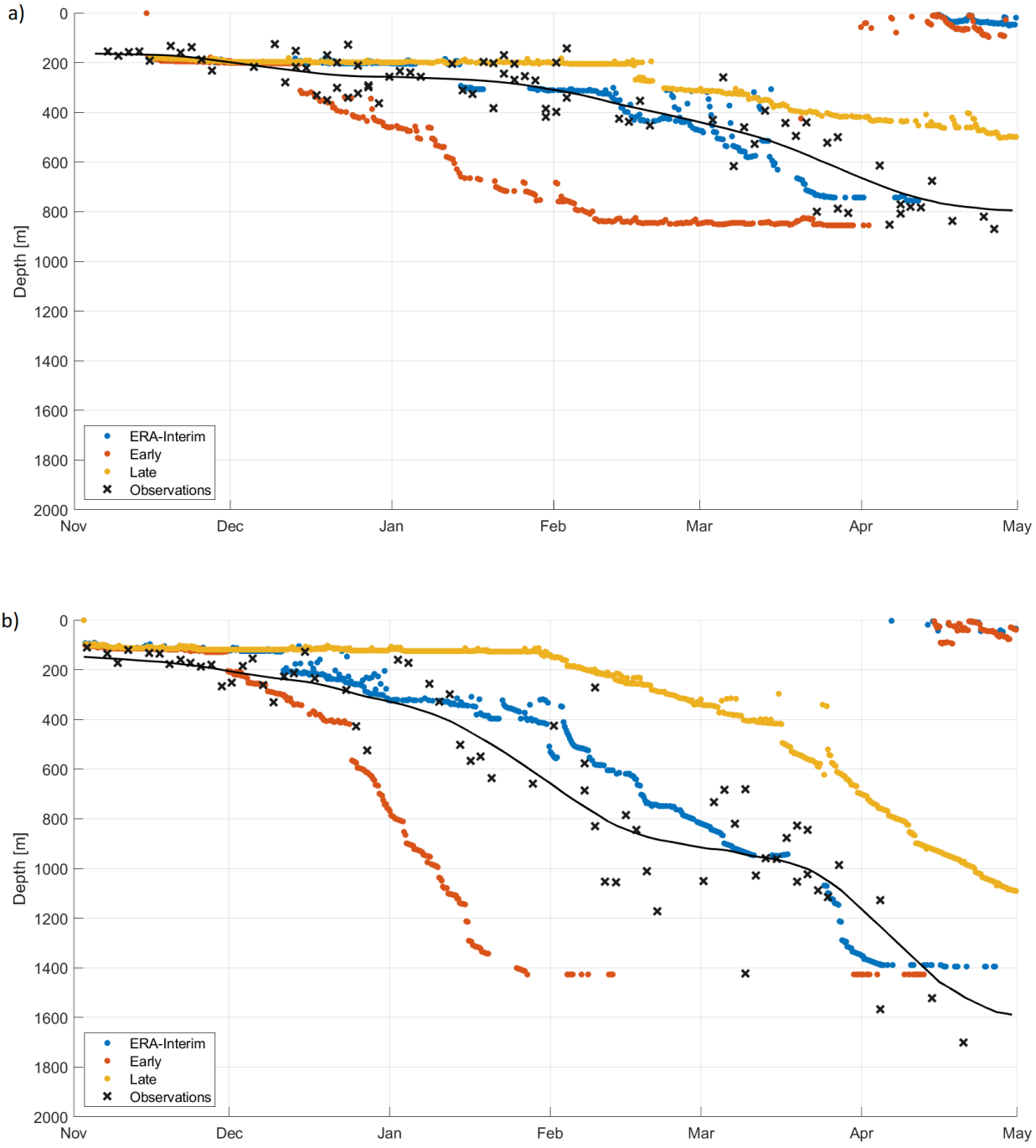

Figure 3.14: Evolution of observed (black crosses) and simulated (colored dots) mixed-layer depth evolution from 2005/2006 (a) and 2007/2008 (b) with different atmospheric forcing (see text for details). The black lines are the 30-days running mean of the observations.

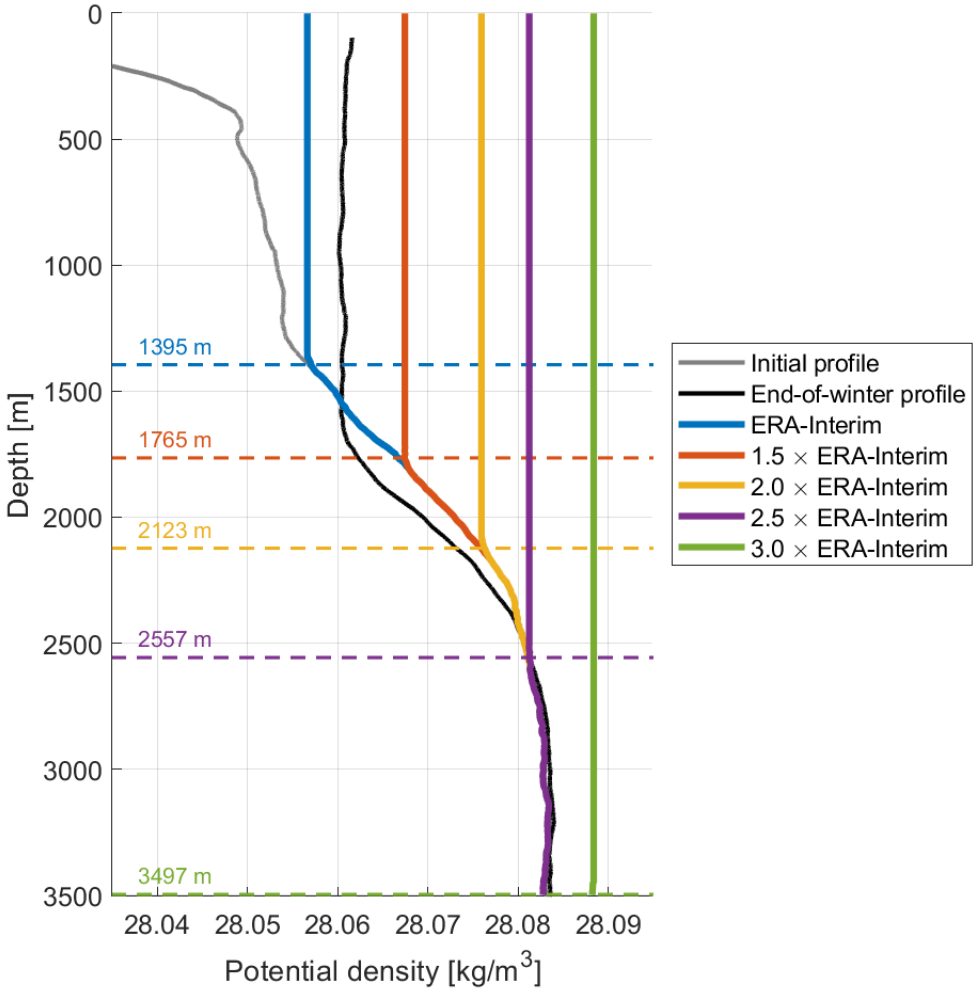

Figure 3.15: End-of-winter density profiles from simulations with different multiples of the actual atmospheric forcing (ERA-Interim). The gray profile represents the initial conditions from 3. November 2007, while the black profile is from 14. April 2008 when the deepest convection that winter was observed (1520 m). The dashed horizontal lines mark the maximum mixed-layer depth from each simulation.

Chapter 4

Discussion and conclusion

Water mass transformation in the Greenland Sea Gyre through the first decade of the 21st century has been an active topic of investigation (e.g. Ronski and Budéus, 2005; Latarius and Quadfasel, 2010, 2016; Brakstad et al., 2019). While these studies mainly focused on interannual variability, the high temporal resolution of the present data set obtained from three moored profilers located within the gyre between 1999 and 2009 also allowed for a more detailed investigation of the mixed-layer evolution through winter and the impact of short, intense atmospheric events.

As documented by previous studies (e.g. Østerhus and Gammelsrød, 1999; Latarius and Quadfasel, 2010; Lauvset et al., 2018; Brakstad et al., 2019), a significantly warming and salinification of the entire water column in the Greenland Sea Gyre was observed. The interannual variability in convection depth through the record depended on heat loss to the atmosphere, the stratification of the water column, and lateral fluxes of heat and freshwater. The evolution of the mixed layer each winter was separated into three distinct phases where most of the mixed-layer cooling took place in the first phase, and the deepening mainly occurred in the second phase. Corroborating the results of Papritz and Spengler (2017), CAOs were responsible for 50-80 % of the total heat loss each winter and were hence of major importance for the end-of-winter convection depths. Even though the total heat loss through the winter was the most important factor determining the resulting convection depth, both the distribution of heat fluxes and the stratification of the water column had significant impact on the convection process.

4.1 Factors affecting the depth of convection

The three main factors determining the depth of convection in the Greenland Sea are heat loss to the atmosphere, stratification of the water column prior to the onset of convection, and lateral fluxes of heat and freshwater.

4.1.1 Atmospheric forcing

Even with favorable conditions, such as a weakly stratified water column, strong atmospheric forcing is required for deep convection to occur (Lauvset et al., 2018; Brakstad et al., 2019). The winters in our record with the weakest atmospheric forcing generally had the shallowest convection (Figure 3.3). Up to 80 % of the total heat loss each winter takes place during CAOs (Table 3.1). Consequently, winters with few CAOs tend to have weak turbulent heat fluxes and relatively shallow convection (Figure 4.1). One winter (2006/2007) stands out from the general pattern in Figure 4.1. This winter was characterized by a strong intermediate stratification in fall which restrained the depth of the mixed layer and convection was therefore shallower than other winters with similar amount of heat loss (Section 3.2).

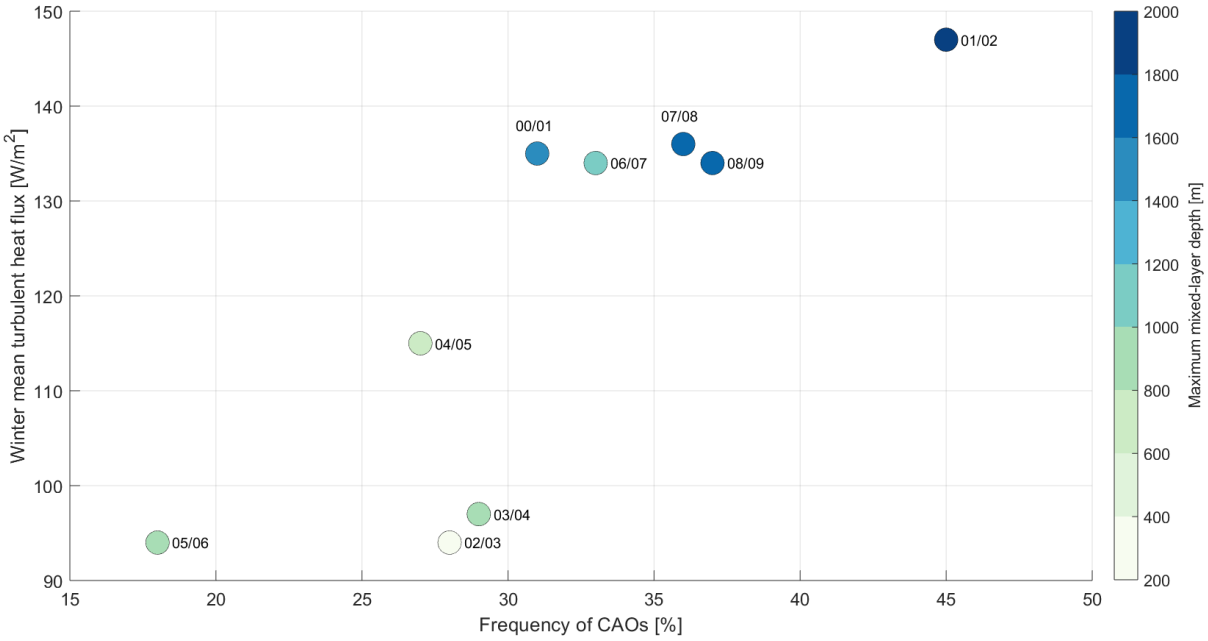

Figure 4.1: Winter mean turbulent heat flux plotted as a function of CAO frequency each winter. The maximum convection depth each winter, determined using data from the profiling moorings and by Brakstad et al. (2019), is shown in color.

4.1.2 Water column stratification and preconditioning

The water column stratification prior to the onset of convection also affects the interannual variability in convections depths (Figure 3.3). A strongly stratified water column in fall restrain the convection depth the subsequent winter (Section 3.2). The stratification in fall is heavily influenced by convective mixing previous winters. Winters with deep convection weakens the stratification and precondition the water column for deep convection the following winter.

The effect of wintertime convection on the water column stratification is clearly visible in the stepwise reduction in intermediate stratification and in the concurrent increase in convection depth

from 2005 to 2008 (Figures 3.2 and 3.3). Between 2002 and 2005 the winter mean turbulent heat flux was relatively low (Table 3.1), and the convection never exceeded 1000 m depth (Figure 4.1 and Brakstad et al., 2019). This led to an intermediate water column stratification that was anomalously strong prior to the winter 2005/2006 (Figure 3.3). Although relatively weak, the atmospheric forcing in 2005/2006 managed to erode through the upper 900 m of the water column, slightly decreasing the intermediate stratification. The enhanced atmospheric forcing in 2006/2007 resulted in even deeper convection and the water column stratification was weakened further. In 2007/2008 the water column was sufficiently preconditioned in fall and the atmospheric forcing was strong enough for the end-of-winter mixed layer to extend to the stability maximum separating the GSAIW from the GSDW at approximately 1500 m depth.

Even the shallowest end-of-winter mixed-layer depths observed in this study were relatively deep compared to the convection depths in the late 1980s and early 1990s which rarely exceeded 300 m (Brakstad et al., 2019). During this period, a pronounced near-surface stratification associated with a fresh surface layer inhibited deep convection. Brakstad et al. (2019) found that when the summer near-surface (upper 50 m) salinity between 1986 and 2016 was lower than the period mean, the late winter mixed-layer depth the following winter did not exceed 300 m, regardless of the magnitude of the surface heat loss (Figure 9 in Brakstad et al., 2019). Since the moored profilers did not measure to the surface, it was not possible to calculate the near-surface salinity. However, according to Brakstad et al. (2019) the near-surface salinity anomaly has remained positive after 1994 and hence all winters covered in this study had a sufficiently saline surface layer for deep convection to occur as long as the heat forcing was strong enough.

4.1.3 Lateral fluxes

In addition to air-sea fluxes the water column in the Greenland Sea is constantly affected by ambient water masses. Eddy fluxes of warm and saline Atlantic-origin water from both the EGC and from the outer NwAC flowing northward along the Mohn and Knipovich Ridges might influence the water column in the gyre (e.g. Latarius and Quadfasel, 2016; Håvik et al., 2017). Voet et al. (2010) argued based on Argo float measurements that the exchange between the NwAC and the Greenland Sea is limited and that most of the lateral fluxes must come from the EGC. Spall (2010), on the other hand, used an idealized numerical model to simulate the circulation in the Nordic Seas and found that the ridge separating the western and eastern basins not completely inhibits exchange between the basins. In addition to eddy fluxes the exchange can take place as flow through deep gaps in the ridge. Not much is known about the nature of these lateral fluxes, but they clearly play an important role in the evolution of the water column in the Greenland Sea through winter. During periods with weak atmospheric forcing it seemed like the lateral flux of heat overcompensated for the surface heat loss such that the water column restratified and the mixed-layer depth shoaled (Figure 3.7a).

4.1.4 Challenges in investigating the effect of atmospheric forcing on short time scales

In addition to the supply of heat through eddy fluxes from the currents surrounding the gyre (e.g. Latarius and Quadfasel, 2016) distinct patches of warm and saline water were observed near the surface in the Greenland Sea. These intrusions made it difficult to analyze the effect of atmospheric forcing on short time scales. The patches, which occupied the surface layer of the water column from one to several days, significantly altered the mixed-layer properties (both increasing stratification, temperature, and salinity). As these changes were not caused by atmospheric interactions, the profiles with such patches were removed (Section 2.4).

4.2 Phases of the convection process

The convection process can be divided into three distinct phases (Section 3.3). During the first phase the mixed layer remains relatively shallow, but cools substantially during periods of strong atmospheric forcing (Figure 3.7). The shallow mixed layer at the beginning of winter requires little heat loss for the entire layer to cool substantially. When the mixed layer becomes dense enough to erode the near-surface stratification, the second phase begins and the mixed-layer depth increases rapidly. The mixed-layer temperature changes little in phase 2 because of the increasing depth. In the third phase the deepening ceases and the mixed-layer depth stabilizes before the water column restratifies. The cessation of mixed-layer deepening occurs late in spring when the atmospheric forcing becomes weaker. Phase 3 was not investigated further in this study due to lack of data.

Periods of strong atmospheric forcing, such as during CAOs, affect the mixed layer differently depending on the phase in which they occur. In the first phase CAOs mostly cool the mixed layer. Later in winter, during the second phase, CAOs deepen the mixed layer extensively (Figure 3.10). In both phases the heat content of the active part of the water column decreases during CAOs (Figure 3.11). The active part of the water column is the part influenced by convection.

4.2.1 Effect of heat loss distribution

From idealized simulations with the one-dimensional mixed-layer model it was evident that the distribution of heat fluxes influences the onset of phase 2 (Figure 3.14). If most of the CAOs takes place early in winter, phase 2 also starts earlier than if most of the CAOs occur later. Different distributions of CAOs may account for some of the interannual variability in the timing of the transition from phase 1 to phase 2 (Figure 3.6). Both for the idealized simulations of winter 2005/2006 and 2007/2008 the end-of-winter convection depth was deepest when the strongest heat fluxes were concentrated early in winter and phase 2 started already in December. Winters with CAOs concentrated in the first half thus seem to be more favorable for deep convection. The reason for this difference is mainly the lateral import of heat. Weak atmospheric heat fluxes early in winter can not compensate for the lateral supply of heat, and not the least cool the mixed layer enough for phase

2 to begin. When the heat fluxes strengthens later in winter, the upper part of the water column is warmer than initially and more cooling is needed to obtain same convection depth compared to when strong atmospheric forcing occurs earlier. This imbalance between atmospheric forcing and lateral fluxes is also evident in the model. In addition, the flux of freshwater that is added to the surface for each iteration of the model increases the surface stratification as it is not mixed down in the water column when the mixed-layer depth remains unchanged.

4.3 Convection to the bottom

The stability maximum that formed in the early 1990s and since then has been separating the product of wintertime convection (GSAIW) from the deeper GSDW was evident around 1500 m throughout the record Figure 3.2. Even though the mixed-layer extended down to the stability maximum several winters (2001/2002, 2007/2008, and 2008/2009), convection never penetrated the maximum. Beneath 2000 m the GSDW is very weakly stratified (Figure 3.13). If the stability maximum was eroded, only a small amount of further forcing would be required for convection to reach the bottom. The amount of additional heat loss required to breach the stability maximum was investigated using the mixed-layer model. When the model was forced with heat fluxes three times the magnitude of the actual forcing the cooling was sufficient for the mixed layer to erode the strong stratification and bottom-reaching convection occurred (Figure 3.15). Since the model generally underestimated the convection depth a slightly lower heat loss might suffice, but the amount of forcing required is still unrealistically high. A three-fold increase in the turbulent heat fluxes over the Greenland Sea in 2007/2008 correspond to a winter mean turbulent heat flux in excess of 400 W/m^2. At least since the 1950s winter mean turbulent heat fluxes higher than 200 W/m^2 have not occurred (Moore et al., 2015).

In addition to heat loss, the stratification of the water column is an important factor in determining the depth of convection. Winters with deep convection weakens the stratification through mixing and preconditions the water column for deep convection subsequent winters. The deep convection in 2007/2008 led to an even more weakly stratified water column in fall 2008/2009 and more favorable conditions for convection. Nevertheless, convection in 2008/2009 also stopped when reaching the stability maximum. If the heat loss in winters after 2008/2009 had been of similar strength as 2007/2008 and 2008/2009, and the convection kept reaching the stability maximum, the water column stratification could become even weaker and perhaps sufficiently preconditioned for bottom-reaching convection to again occur.

However, no matter how weakly stratified the water column is, high heat loss is required to initiate deep convection. From the early 1980s the amount of CAOs, and hence the turbulent heat fluxes in the Greenland Sea, have decreased (Moore et al., 2015; Somavilla, 2019). In the winters following 2008/2009 the mean turbulent heat fluxes have generally been weaker. In winter 2009/2010 no mixed layers deeper than 500 m were observed, and between 2009 and 2016 convection down to the stability maximum occurred only once, in 2010/2011 (Brakstad et al., 2019).

Since 2010/2011 the intermediate stratification has increased (Brakstad et al., 2019). This implies that the odds of bottom-reaching convection occurring in the Greenland Sea in the near future are minimal.

References

Aagaard, K., J. H. Swift, and E. C. Carmack (1985). Thermohaline circulation in the Arctic Mediterranean Seas. *Journal of Geophysical Research 90*(C3), 4833–4846.

Brakstad, A., K. Våge, L. Håvik, and G. W. K. Moore (2019). Water mass transformation in the Greenland Sea during the period 1986-2016. *Journal of Physical Oceanography 49*, 121–140.

Budéus, G., W. Schneider, and G. Krause (1998). Winter convective events and bottom water warming in the Greenland Sea. *Journal of Geophysical Research: Oceans 103*(C9), 18513–18527.

Budéus, G. T. (2009). Autonomous Daily CTD Profiles Between 3,700 Meters and the Ocean Surface. *SeaTechnology* (October 2009), 45–48.

Chafik, L. and T. Rossby (2019). Volume, Heat, and Freshwater Divergences in the Subpolar North Atlantic Suggest the Nordic Seas as Key to the State of the Meridional Overturning Circulation. *Geophysical Research Letters 46*(9), 4799–4808.

Dee, D. P., S. M. Uppala, A. J. Simmons, P. Berrisford, P. Poli, S. Kobayashi, U. Andrae, M. A. Balmaseda, G. Balsamo, P. Bauer, P. Bechtold, A. C. Beljaars, L. van de Berg, J. Bidlot, N. Bormann, C. Delsol, R. Dragani, M. Fuentes, A. J. Geer, L. Haimberger, S. B. Healy, H. Hersbach, E. V. Hólm, L. Isaksen, P. Kållberg, M. Köhler, M. Matricardi, A. P. Mcnally, B. M. Monge-Sanz, J. J. Morcrette, B. K. Park, C. Peubey, P. de Rosnay, C. Tavolato, J. N. Thépaut, and F. Vitart (2011). The ERA-Interim reanalysis: Configuration and performance of the data assimilation system. *Quarterly Journal of the Royal Meteorological Society 137*(656), 553–597.

Dickson, R., J. Lazier, J. Meincke, P. Rhines, and J. Swift (1996). Long-term coordinated changes in the convective activity of the North Atlantic. *Progress in Oceanography 38*(3), 241–295.

Dickson, R. R. and J. Brown (1994). The production of North Atlantic Deep Water: Sources, rates, and pathways. *Journal of Geophysical Research: Oceans 99*(C6), 12319–12341.

Eldevik, T., J. E. Ø. Nilsen, D. Iovino, K. A. Olsson, A. B. Sandø, and H. Drange (2009). Observed sources and variability of Nordic seas overflow. *Nature Geoscience 2*(6), 406–410.

Fletcher, J., S. Mason, and C. Jakob (2016). The climatology, meteorology, and boundary layer structure of marine cold air outbreaks in both hemispheres. *Journal of Climate 29*(6), 1999–2014.

Fogelqvist, E., J. Blindheim, T. Tanhua, S. Østerhus, E. Buch, and F. Rey (2003). Greenland-Scotland overflow studied by hydro-chemical multivariate analysis. *Deep-Sea Research Part I: Oceanographic Research Papers 50*(1), 73–102.

Gascard, J. C., A. J. Watson, M. J. Messlas, K. A. Olsson, T. Johannessen, and K. Simonsen (2002). Long-lived vortices as a mode of deep ventilation in the Greenland Sea. *Nature 416*(6880), 525–527.

Hansen, B., K. M. Husgaro, H. Hátún, and S. Østerhus (2016). A stable Faroe Bank Channel overflow 1995-2015. *Ocean Science 12*(6), 1205–1220.

Hansen, B. and S. Østerhus (2000). North Atlantic-Nordic Seas exchanges. *Progress in Oceanography 45*(2), 109–208.

Harden, B. E., R. S. Pickart, H. Valdimarsson, K. Våge, L. de Steur, C. Richards, F. Bahr, D. Torres, E. Børve, S. Jónsson, A. Macrander, S. Østerhus, L. Håvik, and T. Hattermann (2016). Upstream sources of the Denmark Strait Overflow: Observations from a high-resolution mooring array. *Deep-Sea Research Part I: Oceanographic Research Papers 112*, 94–112.

Håvik, L., R. S. Pickart, K. Våge, D. J. Torres, A. Thurnherr, A. Beszczynska-Möller, W. Walczowski, and W.-J. von Appen (2017). Evolution of the East Greenland Current from Fram Strait to Denmark Strait: Synoptic measurements from summer 2012. *Journal of Geophysical Research: Oceans 122*, 7267–7290.

IOC, SCOR, and IAPSO (2010). The international thermodynamic equation of seawater 2010 : Calculation and use of thermodynamic properties. *Intergovernmental Oceanographic Commission, Manuals and Guides 56*.

IPCC (2014). *Climate Change 2014: Synthesis Report. Contribution of Working Groups I, II and III to the Fifth Assessment Report of the Intergovernmental Panel on Climate Change*.

Jeansson, E., A. Olsen, and S. Jutterström (2017). Arctic Intermediate Water in the Nordic Seas, 1991-2009. *Deep-Sea Research Part I: Oceanographic Research Papers 128*(March 2016), 82–97.

Jónsson, S. and H. Valdimarsson (2004). A new path for the Denmark Strait overflow water from the Iceland Sea to Denmark Strait. *Geophysical Research Letters 31*(3), 2–5.

Karstensen, J., P. Schlosser, D. W. Wallace, J. L. Bullister, and J. Blindheim (2005). Water mass transformation in the Greenland Sea during the 1990s. *Journal of Geophysical Research: Oceans 110*(7), 1–18.

Kolstad, E. W., T. J. Bracegirdle, and I. A. Seierstad (2009). Marine cold-air outbreaks in the North Atlantic: Temporal distribution and associations with large-scale atmospheric circulation. *Climate Dynamics 33*(2-3), 187–197.

Kuhlbrodt, T., A. Griesel, M. Montoya, A. Levermann, M. Hofmann, and S. Rahmstorf (2007). On the driving processes of the Atlantic Meridional Overturning Circulation. *Reviews of Geophysics 45*(2004), RG2001.

Latarius, K. and D. Quadfasel (2010). Seasonal to inter-annual variability of temperature and salinity in the Greenland Sea Gyre: heat and freshwater budgets. *Tellus A: Dynamic Meteorology and Oceanography 62*(4), 497–515.

Latarius, K. and D. Quadfasel (2016). Water mass transformation in the deep basins of the Nordic Seas: Analyses of heat and freshwater budgets. *Deep-Sea Research Part I: Oceanographic Research Papers 114*, 23–42.

Lauvset, S. K., A. Brakstad, K. Våge, A. Olsen, E. Jeansson, and K. A. Mork (2018). Continued warming, salinification and oxygenation of the Greenland Sea gyre. *Tellus A: Dynamic Meteorology and Oceanography 70*(1), 1–9.

Lorbacher, K., D. Dommenget, P. P. Niiler, and A. Köhl (2006). Ocean mixed layer depth: A subsurface proxy of ocean-atmosphere variability. *Journal of Geophysical Research: Oceans 111*(7), 1–22.

Lozier, M. S., F. Li, S. Bacon, F. Bahr, A. S. Bower, S. A. Cunningham, M. F. de Jong, L. de Steur, B. DeYoung, J. Fischer, S. F. Gary, B. J. W. Greenan, N. P. Holliday, A. Houk, L. Houpert, M. E. Inall, W. E. Johns, H. L. Johnson, C. Johnson, J. Karstensen, G. Koman, I. A. Le Bras, X. Lin, N. Mackay, D. P. Marshall, H. Mercier, M. Oltmanns, R. S. Pickart, A. L. Ramsey, D. Rayner, F. Straneo, V. Thierry, D. J. Torres, R. G. Williams, C. Wilson, J. Yang, I. Yashayaev, and J. Zhao (2019). A sea change in our view of overturning in the subpolar North Atlantic. *Science 363*(6426), 516–521.

Malmberg, S. A. (1983). Hydrographic Investigations in the Iceland and Greenland Seas in late Winter 1971. *Jökull*, 133–140.

Marshall, J. and F. Schott (1999). Open-Ocean Convection: observations, theory and models. *Reviews of Geophysics 37*(98), 1–64.

Mastropole, D., R. S. Pickart, H. Valdimarsson, K. Våge, K. Jochumsen, and J. Girton (2017). On the hydrography of Denmark Strait. *Journal of Geophysical Research: Oceans 122*, 306–321.

Mauritzen, C. (1996). Production of dense overflow waters feeding the North Atlantic across the Greenland-Scotland Ridge. Part 1: Evidence for a revised circulation scheme. *Deep-Sea Research Part I: Oceanographic Research Papers 43*(6), 807–835.

Meincke, J., B. Rudels, and H. J. Friedrich (1997). The Arctic Ocean-Nordic Seas thermohaline system. *ICES Journal of Marine Science 54*(3), 283–299.

Messias, M. J., A. J. Watson, T. Johannessen, K. I. Oliver, K. A. Olsson, E. Fogelqvist, J. Olafsson, S. Bacon, J. Balle, N. Bergman, G. Budéus, M. Danielsen, J. C. Gascard, E. Jeansson, S. R. Olafsdottir, K. Simonsen, T. Tanhua, K. Van Scoy, and J. R. Ledwell (2008). The Greenland Sea tracer experiment 1996-2002: Horizontal mixing and transport of Greenland Sea Intermediate Water. *Progress in Oceanography 78*(1), 85–105.

Moore, G. W. K., K. Våge, R. S. Pickart, and I. A. Renfrew (2015). Decreasing intensity of open-ocean convection in the Greenland and Iceland seas. *Nature Climate Change 5*(9), 877–882.

Nilsen, J. E. Ø. and E. Falck (2006). Variations of mixed layer properties in the Norwegian Sea for the period 1948-1999. *Progress in Oceanography 70*(1), 58–90.

Østerhus, S. and T. Gammelsrød (1999). The abyss of the nordic seas is warming. *Journal of Climate 12*(11), 3297–3304.

Østerhus, S., R. Woodgate, H. Valdimarsson, B. Turrell, L. De Steur, D. Quadfasel, S. M. Olsen, M. Moritz, C. M. Lee, K. M. H. Larsen, S. Jónsson, C. Johnson, K. Jochumsen, B. Hansen, B. Curry, S. Cunningham, and B. Berx (2019). Arctic Mediterranean exchanges: A consistent volume budget and trends in transports from two decades of observations. *Ocean Science 15*(2), 379–399.

Papritz, L., S. Pfahl, H. Sodemann, and H. Wernli (2015). A climatology of cold air outbreaks and their impact on air-sea heat fluxes in the high-latitude South Pacific. *Journal of Climate 28*(1), 342–364.

Papritz, L. and H. Sodemann (2018). Characterizing the Local and Intense Water Cycle during a Cold Air Outbreak in the Nordic Seas. *Monthly Weather Review 146*(11), 3567–3588.

Papritz, L. and T. Spengler (2017). A Lagrangian climatology of wintertime cold air outbreaks in the Irminger and Nordic Seas and their role in shaping air-sea heat fluxes. *Journal of Climate 30*(8), 2717–2737.

Pickart, R. S., D. J. Torres, and R. A. Clarke (2002). Hydrography of the Labrador Sea during Active Convection. *Journal of Physical Oceanography 32*(2), 428–457.

Price, J. F., R. A. Weller, and R. Pinkel (1986). Diurnal cycling: Observations and models of the upper ocean response to diurnal heating, cooling, and wind mixing. *Journal of Geophysical Research 91*(C7), 8411.

Rhines, P., S. Häkkinen, and S. A. Josey (2008). *Is oceanic heat transport significant in the climate system? In: Dickson, B., Meincke, J., Rhines, P. (Eds.), Arctic-Subarctic Ocean Fluxes: Defining the Role of the Northern Seas in Climate.*

Ronski, S. and G. Budéus (2005). Time series of winter convection in the Greenland Sea. *Journal of Geophysical Research C: Oceans 110*(4), 1–11.

Rudels, B., D. Quadfasel, H. Friedrich, and M.-N. Houssais (1989). Greenland Sea convection in the winter of 1987-1988. *Journal of Geophysical Research 94*(88), 3223–3227.

Smeed, D. A., S. A. Josey, C. Beaulieu, W. E. Johns, B. I. Moat, E. Frajka-Williams, D. Rayner, C. S. Meinen, M. O. Baringer, H. L. Bryden, and G. D. McCarthy (2018). The North Atlantic Ocean Is in a State of Reduced Overturning. *Geophysical Research Letters 45*(3), 1527–1533.

Somavilla, R. (2019). Draining and Upwelling of Greenland Sea Deep Waters. *Journal of Geophysical Research: Oceans 124*(4), 2842–2860.

Spall, M. A. (2010). Non-local topographic influences on deep convection: An idealized model for the Nordic Seas. *Ocean Modelling 32*(1-2), 72–85.

Srokosz, M. A. and H. L. Bryden (2015). Observing the Atlantic Meridional Overturning Circulation yields a decade of inevitable surprises. *Science 348*(6241).

Strass, V. H., E. Fahrbach, U. Schauer, and L. Sellmann (1993). Formation of Denmark Strait overflow water by mixing in the East Greenland Current. *Journal of Geophysical Research 98*(C4), 6907–6919.

Swift, J. H. and K. Aagaard (1981). Seasonal transitions and water mass formation in the Iceland and Greenland seas. *Deep Sea Research Part A, Oceanographic Research Papers 28*(10), 1107–1129.

Swift, J. H., K. Aagaard, and S. A. Malmberg (1980). The contribution of the Denmark strait overflow to the deep North Atlantic. *Deep Sea Research Part A, Oceanographic Research Papers 27*(1), 29–42.

Våge, K., G. W. Moore, S. Jónsson, and H. Valdimarsson (2015). Water mass transformation in the Iceland Sea. *Deep-Sea Research Part I: Oceanographic Research Papers 101*, 98–109.

Våge, K., R. S. Pickart, M. A. Spall, H. Valdimarsson, S. Jónsson, D. J. Torres, S. Østerhus, and T. Eldevik (2011). Significant role of the North Icelandic Jet in the formation of Denmark Strait overflow water. *Nature Geoscience 4*(10), 723–727.

Voet, G., D. Quadfasel, K. A. Mork, and H. Søiland (2010). The mid-depth circulation of the Nordic Seas derived from profiling float observations. *Tellus, Series A: Dynamic Meteorology and Oceanography 62*(4), 516–529.

Wadhams, P., J. Holfort, E. Hansen, and J. P. Wilkinson (2002). A deep convective chimney in the winter Greenland Sea. *Geophysical Research Letters 29*(10), 3–6.